MICROCOPY RESOLUTION TEST CHART

REPORT DOCUMENTATION PAGE		READ INSTRUCTIONS BEFORE COMPLETING FORM
1. REPORT NUMBER NRL Memorandum Report 4344	**2. GOVT ACCESSION NO.** AD-A096 279	**3. RECIPIENT'S CATALOG NUMBER**
4. TITLE *(and Subtitle)* PLUMEX II: A SECOND SET OF COINCIDENT RADAR AND ROCKET OBSERVATIONS OF EQUATORIAL SPREAD-F		**5. TYPE OF REPORT & PERIOD COVERED** Interim report on a continuing NRL problem.
		6. PERFORMING ORG. REPORT NUMBER NRL-MR-4344
7. AUTHOR(s) E.P. Szuszczewicz, R.T. Tsunoda, R. Narcisi and J.C. Holmes		**8. CONTRACT OR GRANT NUMBER(s)**
9. PERFORMING ORGANIZATION NAME AND ADDRESS Naval Research Laboratory Washington, D.C. 20375		**10. PROGRAM ELEMENT, PROJECT, TASK AREA & WORK UNIT NUMBERS** 61153N; RR033-02-44; 71-0949-0-0, and 71-0950-0-0
11. CONTROLLING OFFICE NAME AND ADDRESS Office of Naval Research Arlington, VA 22217		**12. REPORT DATE** December 1980
		13. NUMBER OF PAGES 82
14. MONITORING AGENCY NAME & ADDRESS*(if different from Controlling Office)* RR03302, I25AAXH RR033024 4, XG40		**15. SECURITY CLASS. *(of this report)*** UNCLASSIFIED
		15a. DECLASSIFICATION/DOWNGRADING SCHEDULE

16. DISTRIBUTION STATEMENT *(of this Report)*

Approved for public release; distribution unlimited.

17. DISTRIBUTION STATEMENT *(of the abstract entered in Block 20, if different from Report)*

19. KEY WORDS *(Continue on reverse side if necessary and identify by block number)*

Measurements of equatorial spread-F
Irregularities
Backscatter plumes

20. ABSTRACT *(Continue on reverse side if necessary and identify by block number)*

PLUMEX II was the second in a two-rocket operation that successfully executed space- and time-coincident measurements of equatorial spread-F. The first launch operation (PLUMEX I) was conducted during the late phase in the development and decay of spread-F; major radar plume features were relatively stable with respect to vertical drifts, and the most intense regions of radar backscatter were beginning to decay. The PLUMEX II conditions were substantially different, with the rocket having been launched into the mid-phase of well-developed spread-F, i.e., a ground-based ionosonde showed full range spread while Altair radar maps of meter-size irregularities displayed backscatter plumes that penetrated to the topside F-layer and continued rising with time. Current analysis of

(Continues)

DD `FORM 1 JAN 73` **1473** EDITION OF 1 NOV 65 IS OBSOLETE
S/N 0102-LF-014-6601

AD-A096279

To: Distribution list for NRL Memorandum Report 4344, "PLUMEX II:
      A Second Set of Coincident Radar and Rocket Observations of
      Equatorial Spread-F," by E.P. Szuszczewicz, J.C. Holmes,
      R.T. Tsunoda, and R. Narcisi, dated December 30, 1980.

The following was inadvertently omitted from page ii:

20. Abstract (Continued)

PLUMEX II results show that F-region irregularities were observed only on the bottomside gradient with $F_s h_{max}$ at 510 km and $N_e^{max} \approx 6(10^5)$ cm^{-3}. Smaller scale irregularities (i.e., small scale structure imbedded in larger scale features) appear less intense than corresponding observations in PLUMEX I. If substantiated by more quantitative analyses, this result could support current interpretations of east-west plume asymmetry which suggests that the western wall of a plume (the PLUMEX I case) is more unstable than its eastern counterpart (the PLUMEX II case). With regard to ion composition, NO$^+$ was the dominant positive-charge component at altitudes below the F-region ledge. Across the ledge and throughout the F-layer up to an apogee of 580 km O$^+$ dominated. The ion results support a model of a Rayleigh-Taylor mode which assumes relatively small depletions originating on the F-ledge with initially small horizontal extent. In this model, the local ion composition will be transported to higher altitudes but molecular ions will not be the dominant positive species.

CONTENTS

Accession For

NTIS GRA&I	X
DTIC TAB	☐
Unannounced	☐
Justification	

By_____

Distribution/

Availability Codes

| Dist | Avail and/or Special |
| A | |

iii

PLUMEX II: A SECOND SET OF COINCIDENT RADAR AND ROCKET OBSERVATIONS OF EQUATORIAL SPREAD-F

I. INTRODUCTION

The coordinated measurements of equatorial spread-F
conducted during July 1979 at the Kwajalein Atoll involved
the launch of two instrumented rocket payloads designed to
probe the detailed "in situ" structure of the turbulent
ionospheric plasma. The first launch operation (PLUMEX I;
17 July 1979; 0031:30.25 LT) was conducted during the late
phase in the development and decay of spread-F. The associated
results and discussions of ground-based and rocket-borne
diagnostics have been presented in companion papers[1,2]. The
second rocket (PLUMEX II: 23 July 1979; 2157:30 LT) was
launched into the mid-phase of well-developed spread-F,
i.e., a ground-based ionosonde showed full frequency and
range spread while the Altair radar maps of meter size
irregularity contours displayed backscatter plumes that
penetrated to the topside F-layer and continued rising with
time. We present here the initial PLUMEX II observations of
radar plumes and the "in situ" measurements of the rocket-
borne plasma probes and mass spectrometer. The results are
then compared with PLUMEX I.

1

II.   EXPERIMENTAL RESULTS

A. Ionospheric Conditions and Radar Maps

By 2000 hr LT on the night of the PLUMEX II launch,
ionograms showed that the virtual height (h'F) of the F-
layer had risen at an average rate of 12 meters/sec to an
altitude of 350 km. At that point vertical drifting ceased
and shortly thereafter full-range spread-F was observed.
The virtual height remained constant until 2130 hr LT, when
upward drifting again commenced at an average rate of 18
meters/sec. With full-range spread-F still in effect and
with the F-layer still drifting at an upward rate near 18
meters/sec the PLUMEX II rocket was launched (0957:30 UT on
day 205; 2157:30, 23 July 1979, LT).

Operating at 155.5 MHz (radar backscatter from 1 m
field-aligned irregularities) the Altair radar executed
consecutive magnetic east-west scans in a plane that included
the upleg penetration of the rocket trajectory. Figure 1
presents the contours of constant backscatter strength[3]
plotted in increments of 10 dB, ranging from 0 dB (domain of
small dots) to 50 dB (solid black). The first panel in
Figure 1 shows backscatter returns extending from 350 to
1000 km, with the most intense region (50 dB level) centered
at 635 km. A measure of horizontal and vertical drift
velocity can be achieved by focussing on features "α" (the
50 dB region at 635 km) and "β" (the 20 dB region at an

2

altitude of 550 km, and 125 km west of Altair in the first panel). In the 135 sec time lapse between the radar measurements in panels 1 and 2, the observations showed that $(V_\alpha$ (hor), V_α (vert)) $\sim$ (290 m/sec, 170 m/sec) and $(V_\beta$ (hor), V_β (vert)) $\sim$ (300 m/sec, 150 m/sec). The results can be interpreted as an average magnetic west-to-east plume drift velocity of 295 m/sec (about 130 m/sec faster than corresponding observations in PLUMEX I) with a corresponding average upward vertical drift velocity equal to 160 m/sec. (Note that ionograms showed h'F moving upward at an average rate of 18 m/sec throughout most of the time encompassed by the radar maps in Figure 1. Therefore, one could conclude that the plume was drifting upward at a rate of 142 m/sec relative to the F-layer bottomside.) In the 124 second interval between panels 2 and 3 the average magnetic west-to-east drift velocity was considerably lower, with a rate at 100 m/sec. During this same interval the average vertical drift velocity increased to 270 m/sec (252 m/sec relative to the bottomside F-region).

B. Rocket Profile and Comparison with Radar

The rocket payload that was launched into the spread-F conditions depicted in Figure 1 carried, among other instruments, a quadrupole ion mass spectrometer and a pair of pulsed plasma probes (See Ref. 2 for instrument details and the payload configuration). The pair of pulsed probes simultaneously tracked ion and electron saturation currents while generating conventional Langmuir probe characteristics[2]. Figure 2 displays the upleg measurements

3

of relative electron density as observed by electron satu-
ration currents I_B^e and corroborated by simultaneously measur-
ed ion saturation currents. Because ion and electron satu-
ration currents have significantly different sensitivities
to velocity, sheath and magnetic field effects, variations
in one polarity current not corroborated by the other were
attributed to the various aspect sensitivities and excluded
from Figure 2. This approach not only facilitates quick-look
analysis and established credibility in the interpretation
of the curves as relative electron density profiles, but also
proved to be a valuable technique for eliminating the other-
wise degrading effects of uncontrolled payload tumple and ACS
jet firings that resulted from the failure of payload sepa-
ration from the rocket motor in PLUMEX II. The ordinate in
Figure 2 has a linear scale for time-after-launch with
altitude superimposed at 50 second increments.

The profile shows that the payload entered the very
bottom of the F-layer at $t \sim 145$ sec ($Z \sim 340$ km), a point
designated "A" in Figure 2. From there to an apogee near
581 km (t = 390 sec) the "in situ" probe measurements revealed
a number of irregular structures, all contiguous and co-
located on the bottomside gradient between points "B" and
"C" in Figure 2. From the F-peak to the topside apogee of
581 km there were no "in situ" observations of macroscale
depletions or smaller scale irregularities as reported in
PLUMEX I (Ref. 1).

The payload's upleg trajectory has been superimposed on
the radar maps in Figure 1. With regions A through E (and

4

their associated times of observation) identified on the panel best matched for time coincidence. A step-wise comparison of "in situ" observations (Fig. 2) with the radar maps shows the following correlations:

Point "A" in Figures 1 and 2 corresponds to the lowest position of the bottomside F-layer, a result which co-locates the very bottom of the F-region radar returns with the very bottom of the F-region ledge. Before PLUMEX I and II (an identical correlation was found in PLUMEX I) there were no data to determine their co-location or lack thereof.

The transition from locations A to B is marked by a 20 dB increase in radar backscatter energy, while region B to C is marked by a relatively constant domain of backscatter energy.

Observations at D and E occur along the eastern "wall" of the plume and encompass an altitude domain stretching from the F-layer peak near 500 km to a topside altitude near the vehicle apogee of 580 km.

Figure 3 presents the up- and downleg profiles of relative electron density as measured by "in situ" probe baseline electron saturation currents. (The integrity of the downleg profile was established by the same procedure utilized in Figure 2.) A comparison of the profiles shows the downleg results more representative of an undisturbed F-region, a result consistent with the rocket's west-to-east movement relative to the radar plume. This relative motion (approximately 160 m/sec) carried the rocket payload into the undisturbed F-region just to the east of the observed

5

radar plume (i.e., into the white region on the eastern edge of the first panel in Figure 1).

A comment is in order with regard to the up- and downleg altitudes that have been superimposed at 50 second intervals in Figure 3. In particular, attention is directed to the locations of the very bottom of the two F-region ledge observations, 340 km upleg and 305 km downleg. Because of the 9° dip in the local geomagnetic field the downleg observation at 650 sec corresponds to 338 km when projected along the magnetic field line to the payload position at 145 sec upleg, a result showing virtually no net movement of the ledge between the up and downleg observations. (We note that at the time of launch ionograms showed h'F rising at an approximate rate of 18 m/sec. This vertical drift then reversed near the middle of the flight, establishing consistency in rocket and ionogram results.)

With regard to ion composition, we note that the molecular ion NO^+ was the dominant positive-charge component at altitudes up to 340 km, the very bottom of the F-region ledge ("A" in Figure 2). At all altitudes above 340 km O^+ was observed to be the dominant ion (See Ref. 4 for detailed ion profiles).

III. CONCLUSIONS AND COMPARISONS WITH PLUMEX I

PLUMEX II was the second in a two-rocket operation that successfully executed space- and time-coincident measurements of equatorial spread-F. Comparison of results and

focus on differences in prevailing ionospheric conditions can be achieved by an analysis of the upleg electron density profiles observed in the two operations (PLUMEX I and II). These profiles are presented in Figure 4 with specific features and conditions of observation listed in Table 1.

TABLE 1

A COMPARISON OF CONDITIONS AND OBSERVATIONS
IN THE DNA/PLUMEX CAMPAIGN

	PLUMEX I	PLUMEX II
Launch Time (LT)	17 July 1979; 0031:30.25	23 July 1979; 2157:30
Spread-F Conditions	Late time; topside radar plume in decay phase	Mid-phase of well-developed spread-F; plumes penetrating to topside and rising with time
$F_2 h_{max}$	375 Km	510 Km
F-bottom	240 Km	340 Km
N_e^{max}	1.3 (10^6) cm^{-3}	$\approx 6(10^5)$ cm^{-3}
L (Gradient scale length)	4.0 Km	8.6 Km
T_e	1350 (± 250)°K	TBD
Dominant F_2 Ion	0^+	0^+
Number of Depletions ($\Delta N_e / N_e^0 \geqslant .60$)	4	Only Bottomside Spread-F
Maximum Depletion ($\Delta N_e / N_e^0$)$_{max}$	0.90	≈ 0.75 (An estimate of bottomside macroscale structure)
"In Situ" Irregularity Strength	$\pm 80\%$ fluctuations on bottomside gradient	Fluctuation levels are much less intense than PLUMEX I
Ion Signatures in Holes	$N^+/0^+$ ratio	None
Plume Penetration by Rocket	Western "wall" and plume "head"	Eastern "wall"

<u>Spread-F conditions</u>. PLUMEX I was conducted during the late phase in the development and decay of spread-F. Specifically, the rocket was launched at 0031:30.25 (LT), a full 3 hrs after the occurrence of full range spread and only 30 minutes before its disappearance from ground-based ionograms. Major plume features were relatively stable with respect to vertical drifts, and the most intense regions of radar backscatter were beginning to decay.

The PLUMEX II conditions were substantially different, with the rocket having been launched into the mid-phase of well-developed spread-F, i.e., a ground-based ionosonde showed full-frequency and range spread while the Altair radar maps of meter size irregularity contours displayed backscatter plumes that penetrated to the topside F-layer and continued rising with time. The payload was launched $1\frac{1}{2}$ hours after the onset of full range spread and an estimated two hours before decay.

<u>F-region profiles and "in situ" irregularities</u>. In the PLUMEX I operation, a number of major depletions ($\Delta N_e/N_e^o \lesssim 0.90$) were distributed throughout the F-region with the F-peak ($F_2 h_{max}$) at 375 Km and $N_e^{max} = 1.3 \ (10^6) \ cm^{-3} \ (\pm 10\%)$. The very bottom of the F-layer (F-bottom) was at 240 km and the macroscopic gradient scale length $L^{-1} = (N_e^o)^{-1} \ dN_e^o/dz$ of the bottomside ledge was 4.0 Km. (The macroscopic L was calculated from a zero-order fit to the bottomside ledge between 10^{-2} and $10^{-1} \ N_e^{max}$.) The electron energy distribution was characterized by $T_e = 1350 \ (\pm 250)^o K$ with no obvious

signatures of energy redistribution in and around the depletions.
The most intense "in situ" irregularities (i.e., smaller
scale structure imbedded in the larger scale depletions)
occurred near 275 km on the bottomside ledge ($\pm$ 80% fluctuations
about an estimate N_e^o). The power spectral density in this
region of intense irregularities on the bottomside was
dominated by a $k^{-2.5}$ power law[2] over the intermediate wave-
length domain $k = 2\pi/1$ km to $k = 2\pi/25$ m. This result
supports the role of the collisional Rayleigh-Taylor instability
in generating intermediate wavelength irregularities[2,5,6]
during the occurrence of equatorial spread-F (See References
1 and 2 for additional details.)

The PLUMEX II data have not received the same level
of analysis already applied to the first operation, a result
largely due to the complications of uncontrolled payload tumble
and ACS jet firings that arose from a subsystem failure to
separate the science payload from the second stage rocket
motor. However, there are a number of conclusions that can
be drawn at this time. In the upleg density profile of the
PLUMEX II flight (Fig. 2), F-region irregularities were
observed only on the bottomside gradient, with the F-peak
($F_2 h_{max}$) at 510 km and $N_e^{max} \sim 6(10^5)$ cm^{-3}. In PLUMEX II the
bottomside gradient was substantially softer than in PLUMEX I
with F-bottom at 340 km and L = 8.6 km. A review of analog
records (uncorrected for tumble and jet firings) indicates
that smaller scale "in situ" irregularities were much less
intense than corresponding observations in PLUMEX I. This

result could support current interpretations (e.g., Ref. 7)
of east-west plume asymmetry which suggest that the western
wall of a plume (the PLUMES I case) is more unstable than
its eastern counterpart (the PLUMEX II case).

Ion composition. PLUMEX I and II provided the very
first vertical profiles of ion composition during the occurrence
of equatorial spread-F. The data are particularly relevant
to the subject of plasma bubble formation, vertical transport
and ion signatures of source domains for topside F-region
depletions. Previous "in situ" measurements of ion composition
within plasma depletions came only from satellite-borne mass
spectrometers[8-10] with results that suggested that topside
holes formed at lower altitudes, where $[NO^+]$, $[O_2^+] > [O^+]$,
and rise to greater heights maintaining (to first-order)
their original ion composition. In a final analysis, the
composition can be different because of dependence on the
bubble formation process, the source domain and the bubble
age as manifested by time-dependent chemical processes.

In both PLUMEX operations O^+ was the dominant F-region
ion down to the very bottom of the F-ledge (F-bottom). At
altitudes below F-bottom, molecular ions dominated with a
scale height approaching infinity. (Detailed ion chemical
results and analyses th t go beyond discussions presented
here are available in Reference 4.) The connection of
this observation to topside bubbles and instability mechanisms
is as follows:

The Rayleigh-Taylor and $\bar{E} \times \bar{B}$ gradient drift instabilities, which have been proposed for bubble formation, require a steep bottomside gradient. However, the PLUMEX results show that the molecular ions are dominant only at altitudes below the bottomside F-region gradient, where scale heights are very large and inhibit the instability process. If the bubble does indeed form on the F-region ledge, and if it transports only local ions to higher altitudes, then molecular ions will never dominate topside depletions. This apparent dichotomy has a number of explanations:

(a) Relatively small depletions (i.e., $\Delta N_e / N_e^o \lesssim 0.9$) originating on the F-ledge with initially small horizontal extent can transport the local ion composition to higher altitudes by the Rayleigh-Taylor process; but molecular ions will not be the dominant positive species. Instead, the $[N^+]/[O^+]$ ratio will indicate the original source domain as suggested by McClure et al.[8] and Szuszczewicz et al.[1], and discussed in detail by Narcisi and Szuszczewicz[4].

(b) For molecular ions to be dominant in a topside F-region depletion it appears that one of two mechanisms must apply: (i) An initially small depletion (i.e., $\Delta N_e / N_e^o \lesssim 0.9$) of large horizontal scale size can result in much higher depletion levels (e.g., References 8-10) by fringing fields that drawup the lower densities and molecular ions that populate altitude regimes lower than the sight of the initial perturbation. This mechanism has been studied by Zalesak and Ossakov[11] and appears in substantial agreement with observations.

11

(c) An alternate mechanism for molecular ion dominance
in topside depletions has been proposed by Chiu and Straus[12].
They suggest that plasma bubbles in the nighttime equatorial
ionosphere originate as wind driven waves at one of the
highly variable density gradients below 200 km, rather than
at the bottomside F-region ledge. Once the bubble is formed,
with the low densities and molecular ion dominance characterized
by the lower altitude, it can propogate into the bottomside
F-region and provide the initial perturbation required for
the onset of the Rayleigh-Taylor mode[13-15].

Current analyses of PLUMEX ion composition results
support conclusion "a" as the operating principle on the
nights of "in situ" investigations. This does not negate
"b" and "c" as candidates for other conditions, but it does
leave open the question for further experimental tests.

ACKNOWLEDGMENTS

team contributed significantly to the success of the
rocket-borne plasma probe and mass spectrometer experiments.
Development of the plasma probe technique was provided by
the Office of Naval Research under Work Unit A02-11.11 (71-
0949-0-0), Ionospheric and Stratospheric Interactions, Task
Area RR 043-02-044.

5. Keskinen, M.J., S.L. Ossakow and P.K. Chaturvedi, "Preliminary report on numerical simulations of intermediate wavelength collisional Rayleigh-Taylor instability in equatorial spread-F," J. Geophys. Res. 85, 1775 (1980).

6. Keskinen, M.J., E.P. Szuszczewicz, S.L. Ossakow and J.C. Holmes, "Nonlinear theory and experimental observations of the local collissional Rayleigh-Taylor instability in a descending equatorial spread-F ionosphere," J. Geophys. Res. (Oct. 1980 submitted).

7. Tsunoda, R.T., "Time evolution and dynamics of equatorial backscatter plumes - Growth phase," SRI International Rpt (in press, 1980).

8. McClure, J.P., W.B. Hanson and J.H. Hoffman, "Plasma bubbles and irregularities in the equatorial ionosphere," J. Geophys. Res. 82, 2650 (1977).

9. Brinton, H.C., H.G. Mayr, and G.F. Newton, "Ion composition in the nighttime equatorial F-region: Implications for chemistry and dynamics", (abstract), EOS Trans. AGU, 56, 1038, (1975).

10. Szuszczewicz, E.P., "Ionospheric holes and equatorial spread-F: Chemistry and transport," J. Geophys. Res. 83, 2665, (1978).

11. Zalesak, S.T., and S.L. Ossakow, "Nonlinear equatorial spread F: Spatially large bubbles resulting from large horizontal scale initial perturbations," NRL Memorandum Rpt 4154 (February 6, 1980); J. Geophys. Res. 85, 2131, (1980).

12. Chiu, Y.T. and J.M. Straus, "Rayleigh-Taylor and wind-driven instabilities of the nighttime equatorial ionosphere," J. Geophys. Res. 84, 3283 (1979).

13. Scannapieco, A.J., and S.L. Ossakov, "Nonlinear equatorial spread-F," Geophys. Res. Lett. 3, 451 (1976).

14. Ott, E., "Theory of Rayleigh-Taylor bubbles in the equatorial ionosphere," J. Geophys. Res. 83, 2066 (1978).

15. Chaturvedi, P.K., and S.L. Ossakov, "Nonlinear theory of the collisional Rayleigh-Taylor instability in equatorial spread-F," Geophys. Res. Lett. 4, 558 (1977).
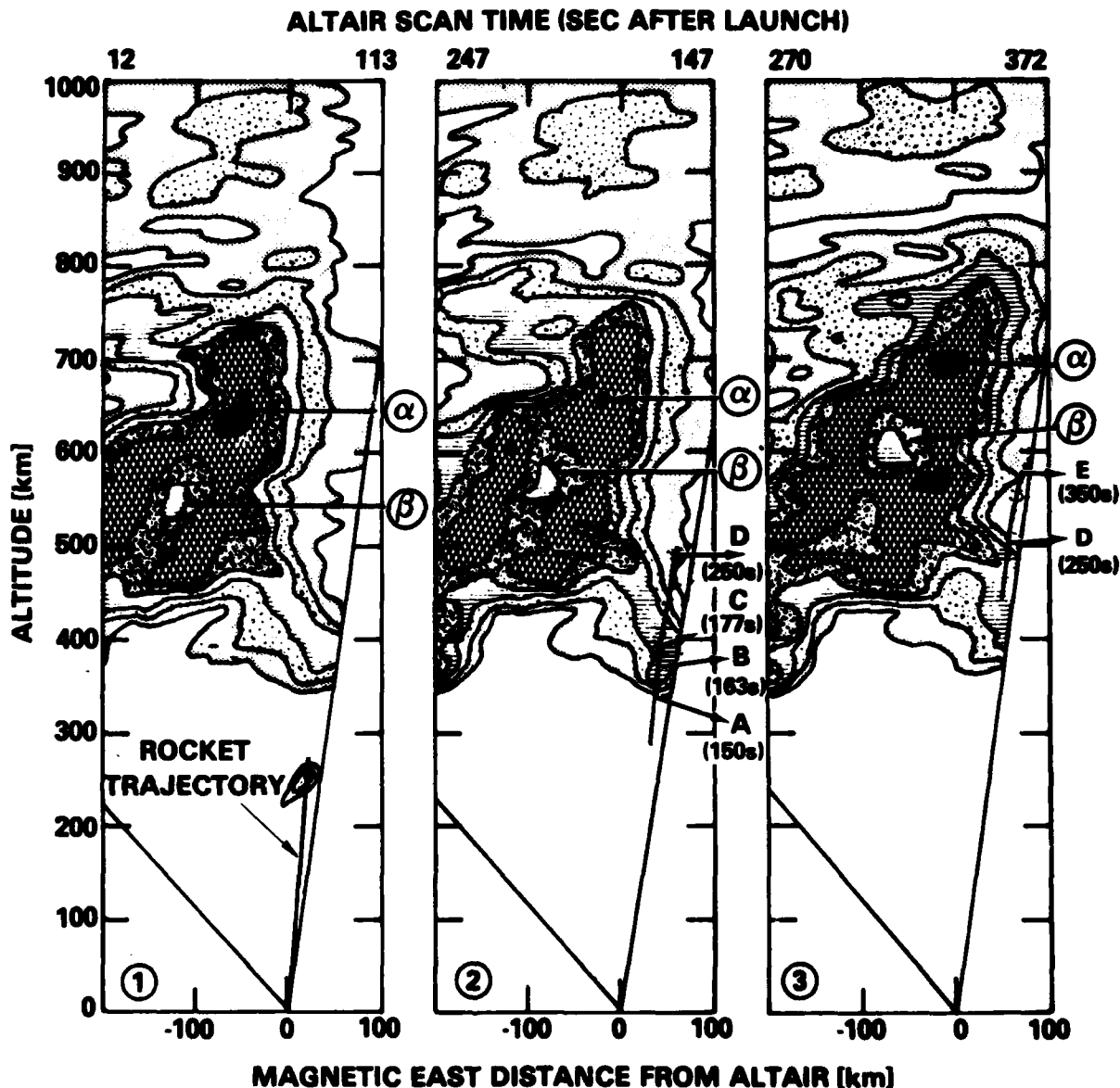
Fig. 1 - Backscatter intensity contour maps (contours are in 10 dB increments with darkest domain, e.g., α , at the 50 dB level) with superposition of the rocket trajectory. The times identified with observations "A" through "F" are included for a more complete representation of temporal correlation with the successive radar scans. Domains "α" and "β" are references for plume dynamics (see text).
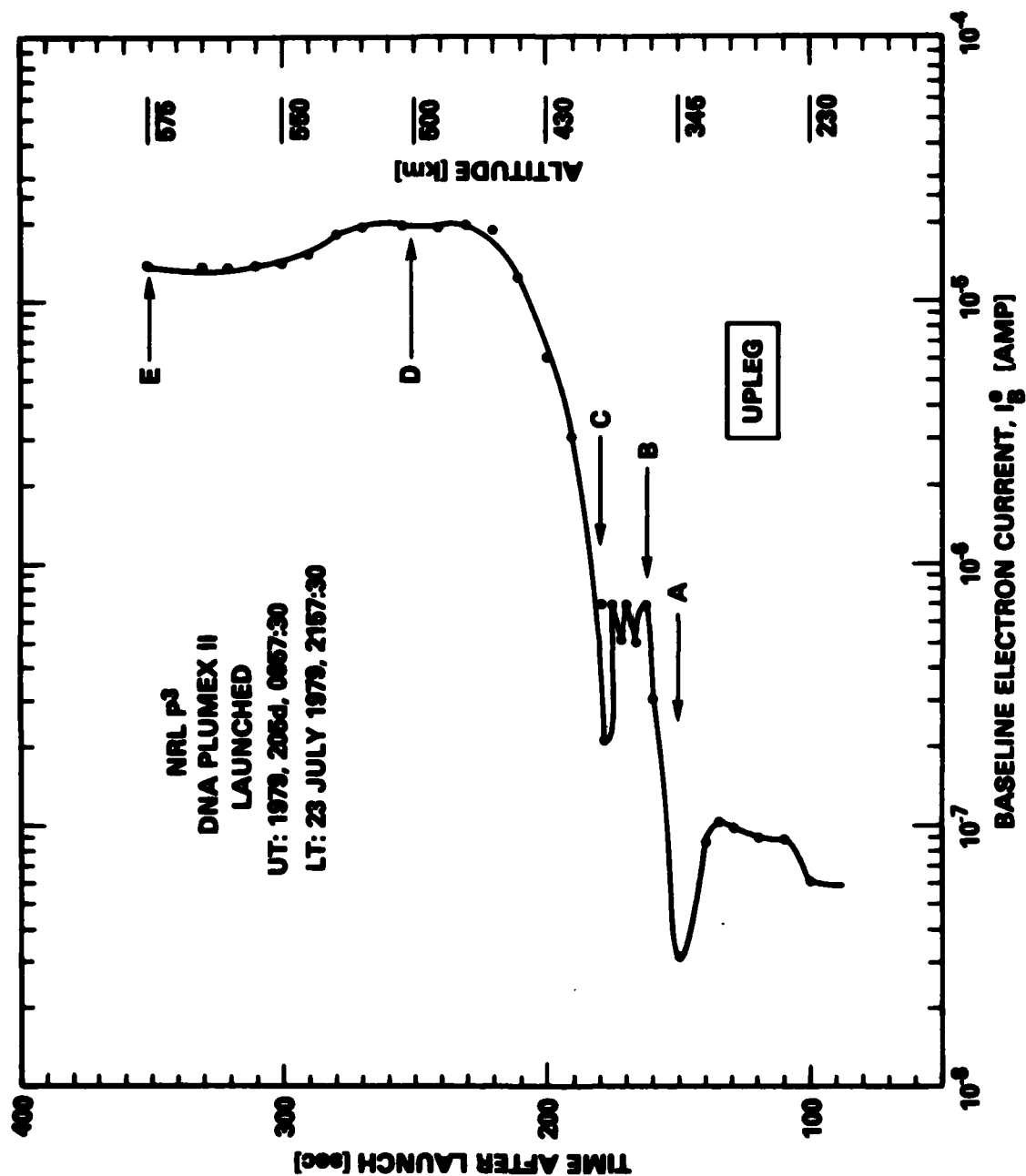
Fig. 2 — Relative electron density profile as measures simultaneously by ion and electron saturation probe currents collected on the upleg trajectory.
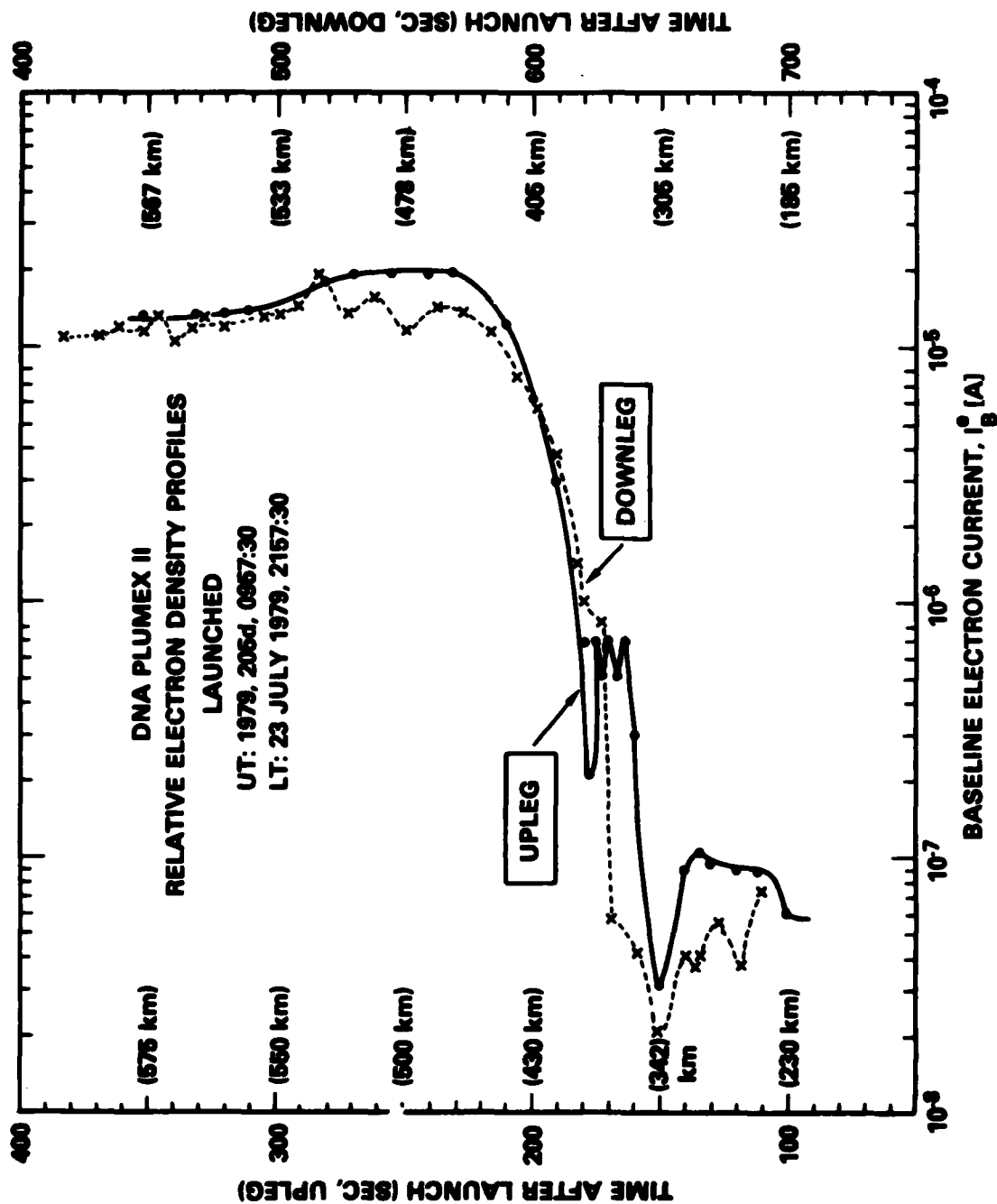
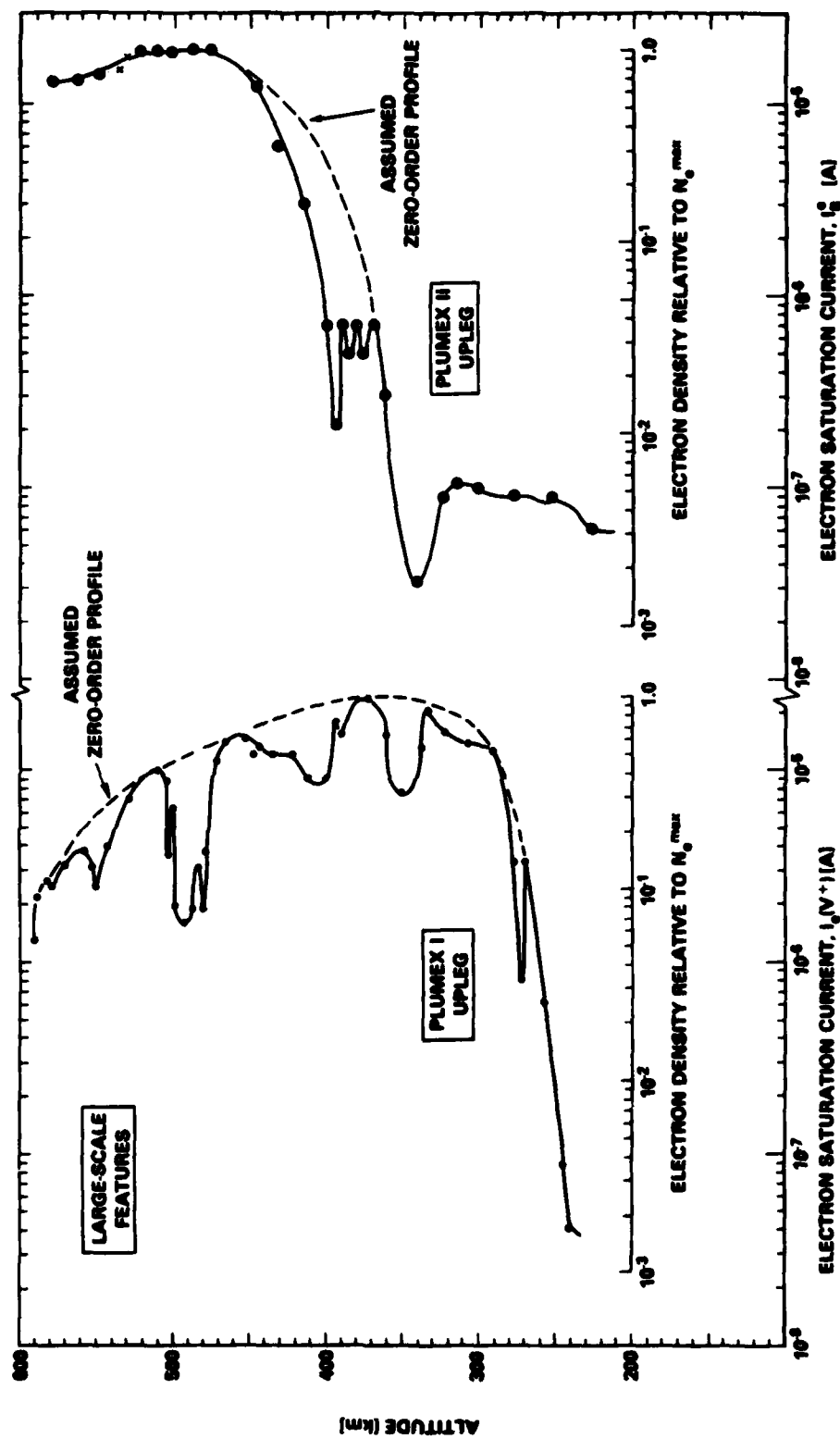Fig. 3 — Comparison of up- and downleg plasma profiles.

Fig. 4 — Comparison of F-region profiles in PLUMEX I and II.

PLUMEX I:
Coincident Radar and Rocket Observations of
Equatorial Spread-F

E. P. Szuszczewicz

E. O. Hulburt Center for Space Research

R. T. Tsunoda

SRI International
Menlo Park, CA 94075

R. Narcisi

Hanscom Air Force Base
Bedford, MA 01731

J. C. Holmes

E. O. Hulburt Center for Space Research

March 17, 1980

NAVAL RESEARCH LABORATORY
Washington, D.C.

REPORT DOCUMENTATION PAGE		READ INSTRUCTIONS BEFORE COMPLETING FORM
1. REPORT NUMBER NRL Memorandum Report 4201	2. GOVT ACCESSION NO.	3. RECIPIENT'S CATALOG NUMBER
4. TITLE (and Subtitle) PLUMEX I: COINCIDENT RADAR AND ROCKET OBSER-VATIONS OF EQUATORIAL SPREAD-F		5. TYPE OF REPORT & PERIOD COVERED Interim report on a continuing DNA problem.
		6. PERFORMING ORG. REPORT NUMBER
7. AUTHOR(s) E. P. Szuszczewicz, R. T. Tsunoda*, R. Narcisi†, and J. C. Holmes		8. CONTRACT OR GRANT NUMBER(s)
9. PERFORMING ORGANIZATION NAME AND ADDRESS Naval Research Laboratory Washington, DC 20375		10. PROGRAM ELEMENT, PROJECT, TASK AREA & WORK UNIT NUMBERS 61153N; RR033-02-44; 71-0949-0-0; DNA Subtask I25AAXHX640
11. CONTROLLING OFFICE NAME AND ADDRESS Office of Naval Research Arlington, Virginia 22217		12. REPORT DATE March 17, 1980
		13. NUMBER OF PAGES 28
14. MONITORING AGENCY NAME & ADDRESS(if different from Controlling Office)		15. SECURITY CLASS. (of this report) UNCLASSIFIED
		15a. DECLASSIFICATION/DOWNGRADING SCHEDULE

16. DISTRIBUTION STATEMENT (of this Report)

Approved for public release; distribution unlimited.

17. DISTRIBUTION STATEMENT (of the abstract entered in Block 20, if different from Report)

19. KEY WORDS (Continue on reverse side if necessary and identify by block number)

Ionosphere
Electron density
Spread-F
In situ measurements

20. ABSTRACT (Continue on reverse side if necessary and identify by block number)

Coordinated measurements of equatorial spread-F conducted during July 1979 at the Kwajalein Atoll have yielded the first definitive space- and time coincident radar and rocket observations of small scale irregularities and large scale plasma depletions. The results have shown that:

(a) Within a large-scale topside F-layer depletion radar backscatter energy is at a level much lower than that observed on the depletion's topside. The same is true of "in situ" irregularity observations, and

(Continues)

20. Abstract (Continued)

(b) Ion composition within a topside depletion can provide signatures of its bottomside source domain and estimates of average maximum vertical drift velocity. For long-lived depletions, molecular-ion signatures (NO^+ and O_2^+) can be lost while bottomside levels of N^+ can be maintained when $[O^+] \approx N_e \gg [NO^+] + [O_2^+]$, and finally,

(c) Large scale fluctuations of O^+ accompanied by a near-constant level of NO^+ and O_2^+ on the bottomside F-layer gradient suggests that neutral atmospheric turbulence is not a major source for bottomside ionospheric plasma irregularities.

PART II
CONTENTS

I. INTRODUCTION

Accumulated information regarding equatorial spread-F phenomena has pointed toward a definite causal relationship between the large scale depletions (also referred to as holes, bite-outs, or bubbles) and range-time-intensity observations of large ionospheric domains with strong radar backscatter returns from the much smaller (meter size) irregularities (called plumes). Woodman and LaHoz (1976) and Kelly, et al. (1976), have suggested that a plume was due to a rising bubble leaving behind a wake of short wave-length irregularities. Another proposal (Szuszczewicz, 1978), arising from considerations of chemistry and transport, suggested that the radar returns originate across the density gradients at the boundaries of large scale depletions. This concept is supported by the work of Ossakow, et al. (1979) where it is inferred that a bubble rising through the F-layer will bifurcate on its topside and produce shorter and shorter wavelength irregularities, either by a cascade or two-step mechanism. Experimental evidence to verify this position has come from an Altair radar experiment (Tsunoda, 1980a) which showed that backscatter maxima tend to occur at altitudes corresponding either to the electron density minima or the upper wall of the plasma depletion. More recently, Tsunoda (1980b) concluded that during the decay phase of meter scale backscatter plumes, the radar returns were maximum on the upper walls of the plasma depletions.

Efforts to examine the exact relationship between radar plumes and ionospheric depletions by performing simultaneous "in situ" and ground-based radar observations (Kelly, et al. 1976; Morse, et al. 1977) have been limited to conditions of bottomside spread-F and required extrapolations in space and time to establish correlations. As expected for bottomside spread-F, the "in situ" probes only observed plasma fluctuations along the portion of the trajectory below the F-layer peak density while the ionosphere above the peak was quite smooth.

The ion composition within the depletions has also been the subject of a number of investigations. Typically, satellite mass spectrometric observations (Brinton et al. 1975; McClure et al, 1977; Szuszczewicz, 1978) have shown that the ion composition can be vastly different inside and outside the bite-outs. Fe^+ ions may be enhanced or depleted, with molecular ions usually more abundant inside the bite-out. Brinton et al. (1975) and McClure et al. (1977) have found O^+ depleted by as much as a factor of 10^3 to a concentration below that of NO^+. The molecular ion NO^+ was found to be dominant in the O^+ depleted region, with the bite-outs varying from a few kilometers to tens of kilometers in width. An analysis of the Atmospheric Explorer-C data (Szuszczewicz, 1978) suggested that a given chemical volume on the bottomside F-layer ($[NO^+]$, $[O_2^+] > [O^+]$) could move upward through a stationary neutral atmosphere and

appear at higher altitudes as a bite-out in the local plasma density. As the bottomside F-region plasma cell moved upward, the relative magnitudes of its ionic components would depend on transit time and on altitude through the height distribution of the neutral gases. This model was consistent with the satellite observations as well as the computational work of Scannapieco and Ossakow (1976).

In a continuing effort to understand the detailed relationships involving large scale plasma depletions, meter-size irregularities and associated ion-chemical signatures, a rocket payload instrumented with a plasma diagnostics complement (plasma probes, electric field sensors, mass spectrometer and a two-frequency beacon experiment) was launched into the topside F-region ionosphere above Roi-Namur in the Kwajalein Atoll (4.3° N dip latitude). The investigation was part of a major effort which coordinated rocket and Altair radar observations with bottomside soundings and ground-based photometric measurements of F-region winds. We present here the initial coordinated observations of the radar plumes and the "in situ" measurements of the rocket-borne plasma probes and mass spectrometer.

II. EXPERIMENTAL RESULTS

A. Ionospheric Conditions and Radar Maps

By 2100 hr LT on the night of the rocket launch, ionograms showed that the nominal bottomside of the F-layer had risen to an altitude of 400 km. At that point, the F-

layer began drifting downward with an almost immediate occurrence of spread-F. The downward drifting continued (as did the spread-F) at an approximate average velocity of 10m/sec with the bottomside F-layer having descended to an altitude near 270 km when the rocket was launched (12:31:30 UT on day 198; 00:31:30, 17 July 1979, LT).

Operating at 155.5 Mhz radar backscatter returns from 1 m ionospheric irregularities) the Altair radar executed consecutive east-west scans in a plane that included the penetration of the rocket's upleg trajectory. Figure 1 presents the contours of constant backscatter strength plotted in 10 dB increments. (For details of the Altair system see Tsunoda et al., 1979). The first panel in Figure 1 shows a backscatter plume just moving out of the radar's eastern-most field of view. That plume, with its highest and most intense backscatter region near 510 km, is connected to backscatter domains extending down to the bottomside of the F-layer. The second panel, with a center scan time 137 seconds later than the first, shows the intense backscatter region further to the east, having drifted there with an approximate west-east velocity of 160m/sec. In the third panel the plume has nearly moved completely out of the radar's field of view and the intense region near 510 km has decayed.

B.   <u>Rocket Profile and Comparison with Radar</u>

The rocket payload that was launched into the spread-F conditions depicted in Figure 1 carried a quadrupole ion

mass spectrometer (from the Air Force Geophysics Laboratory)
a pair of pulsed plasma probes (from the Naval Research
Laboratory), vector electric field sensors (from Utah State
University) and a two-frequency beacon experiment (SRI
International). The pair of pulsed probes simultaneously
tracked ion and electron saturation currents while generating
conventional Langmuir probe characteristics (see e.g.,
Szuszczewicz and Holmes, (1977). Figure 2 displays the upleg
measurements of relative electron density as presented by
correlated ion and electron saturation currents. The
ordinate has a linear scale for time-after-launch with
altitude superimposed at 50 second increments. (Because ion
and electron saturation currents have significantly different
sensitivities to velocity, sheath and magnetic field effects
(e.g., Szuszczewicz and Takacs, 1979) data points not corroborated
by both polarity currents were attributed to the various
aspect sensitivities and therefore were not included in
Figure 1. This approach facilitates quick look analysis and
establishes credibility in the interpretation of the curves
as relative electron density profiles.)

The profile shows that the payload entered the very
bottom of the F-layer at $t \overset{\sim}{=} 103$ sec ($z \overset{\sim}{=} 240$ km). From that
point, to an apogee near 590 km, the "in situ" measurements
revealed a number of plasma depletions depicted in the
figure as regions C, D-E, F-G, H-I, and J-K. The largest
depletion was in region H-I where $\Delta N_e / N_e^O \overset{\sim}{=} 0.85$ with a half-

minimum vertical extent approximatley equal to 23 km.

In the regions of the large-scale depletions, the "in situ" measurements also revealed much smaller scale irregularities. The central plot of "irregularity intensity" in Figure 2 identifies the regions of smaller irregularities and attempts to establish a preliminary quantification for their intensity. ("Irregularity intensities" were scaled directly from probe current fluctuations about an estimated mean. As an illustration, the -4.5 to +4.5 irregularity intensity within region C represents a factor of 9 in the largest peak-to-peak fluctuation measured in that region. (If vehicle potential, plasma temperature and ion composition were constant during the irregularity measurements, then $I \propto N_e$.) More quantitative analyses along with power spectral densities will be determined for future publication.) The results show that the most intense irregularities occurred on the bottomside gradient (region C) with corresponding measurements at all other altitudes at a much lower level. We note that the fluctuations in the largest depletion (region H-I) are smaller than those at "C". The data also indicate that the more intense fluctuations occur on positive density gradients (C,D,E, and I).

The payload's upleg trajectory has been superimposed on the radar maps in Figure 1 with domains A through K (and their associated times of observation) identified on

the panel best matched for time coincidence with the radar results. A step-wise comparison of "in situ" irregularity observations (Fig. 2) with the radar maps reveals some interesting correlations:

Point "A" corresponds to the lowest position of the bottomside F-layer, while "B" is midway up the steep bottomside and very near the point of maximum positive density gradient. Region "C" is at the boundary of the third highest backscatter level (30 dB), and appears to represent the mid-phase development of large scale Rayleigh-Taylor turbulence. Observations at "D", "E", "F" and "G" occur along the western "wall" of the plume, and encompass an altitude domain identified with the F-layer peak. Point "G" represents the payload's entry into the large scale depletion centered near 240 sec (490 km) on the upleg trajectory. The payload's transit from "G" to "I" is marked by a positive gradient in backscatter radar energy, with the maximum return occurring on the topside (region "I" and above) of the H-I depletion. Above the large scale depletion, observations "K" and "J" begin to track the western "wall" of the plume in the topside F-region.

C. Ion Composition

O^+ was observed to be the dominant ion component through-out the entire F-region. From points of view focussed on turbulence and transport the chemical constituency of two regions are worthy of note:

In the H-I depletion on the topside F-layer the major observed ion components were $[O^+] \simeq 0.998\ N_e$, $[N^+] \simeq 0.002\ N_e$ and $([NO^+] + [O_2^+]) < 10^{-4} N_e$. In the adjacent domains there was a different distribution of ions, i.e., outside the depletion we found $[O^+] \simeq 0.992\ N_e$, $[N^+] \simeq 0.007\ N_e$ and $([NO^+] + [O_2^+]) < 2\ (10^{-5})\ N_e$, a distribution typical of the zero-order ionosphere at those altitudes.

The ion composition within the H-I depletion suggests that it may have originated at or near the bottomside F-region where $[O^+] \simeq [O^+]_{H-I}$. Such a region exists at 112 sec ($Z \simeq 262$ km) on the upleg trajectory where it was observed that $[NO^+]$ and $[O_2^+]$ were 1-2% of N_e and the $[O^+]/[N^+]$ ratio was nearly identical to that observed in the H-I domain. This points to N^+ as a long-lived tracer ion for bottomside source regions of topside depletions. The fact that the source region levels of NO^+ and O_2^+ have not been preserved in the topside hole results from their losses by dissociative recombination and a simultaneous loss in production by ion-atom interchange and charge exchange reactions since $[N_2]$ and $[O_2]$ decrease markedly with altitude. The longer it takes a bottomside depletion to move upward into the topside F-layer, the more likely the elimination of molecular ion signatures when $[O^+] \simeq N_e >([NO^+] + [O_2^+])$. In the case of the H-I depletion, a vertical transport time greater than 360 seconds would account for the molecular ion deficiency. (To arrive at this estimate we assumed an instaneous dis-placement of the bottomside ion composition to the H-I

altitude and calculated that in about 6 minutes the molecular ions would decrease to a concentration less than 5 cm^{-3}.) This time estimate suggests an upper limit of about 600 m/sec for the depletion's average vertical drift velocity, a value which is consistent with the wide range in predicted bubble rise velocities (Ossakow and Chaturvedi, 1978; Ossakow et al., 1979; Anderson and Haerendel, 1979). (While this conclusion is correct in its own right, we note that Altair data prior to that shown in Fig. 1 reveal that the backscatter plume was at the nominal altitude shown in Figure 1 for more than 30 minutes.)

The second region of special note is "C" where it was observed that O^+ followed the intense plasma density fluctuations while the molecular ions NO^+ and O_2^+ (representing @0.5-1.0% N_e) did not. Such a result has a possible explanation in an assumption that requires steady state chemical equilibrium in an O^+ dominant domain. (Molecular ions in region "C" can achieve equilibrium concentrations in less than 10 minutes.) Under this condition, molecular ion concentrations are independent of O^+ and vary only with the scale height of the neutral atmospheric constituents N_2 and O_2. The observations conform to this model with a standard zero-order atmospheric distribution, suggesting that neutral atmospheric turbulence is not a major source for the observed plasma fluctuations on the bottomside F-region.

D. North-South Extent of the Depletions

Figure 3 presents the up- and downleg profiles of
relative electron density as measured by "in situ" probe
electron-saturation currents. (The integrity of the downleg
profile was established by the same procedure utilized in
Figure 2.) A comparison of the profiles shows very good
agreement in the two observations of plasma depletions.
Attention is directed to the large scale depletion of the
topside (region H-I):

The up- and downleg measurements of the large topside
hole were separated in time by approximately 340 seconds and
in range by 112 km. During this 340 second interval Altair
radar measurements of plume movement showed an average
easterly drift at a 160 m/sec rate resulting in a total
eastward displacement of 54 km. Adding 14 km to account for
depletion alignment along the magnetic meridian (9°E of true
azimuth) yields a calculated total E-W displacement of 68 km
between the times of the two rocket observations of the
hole. During this time interval the payload had an eastward
range velocity approximately equal to 215 m/sec, resulting
in an east-west separation in the up- and downleg observations
of region H-I equal to 73 km. From this we can conclude
near-perfect up- and downleg targeting of the hole. The
agreement in the two observations of the H-I domain there-
fore suggests that the depletion is aligned with the magnetic
field for at least 112 km. (Parallel arguments dealing with
the depletion at $(t,z) \simeq (153s, 350$ km) would suggest a
field alignment at least as great as 163 km, while the

radar observations of Tsunoda [1980b] showed plasma bubble alignment can extend to 1100 km.)

III. COMMENTS AND CONCLUSIONS

Space- and time coincident measurements of equatorial spread-F conducted during July 1979 at the Kwajalein Atoll have yielded the first definitive observations of small scale irregularities (@1 meter) and large scale plasma depletions as measured independently throughout the F-region by ground-based radar and "in situ" plasma instrumentation. Preliminary analysis of the results leads to the following comments and conclusions:

(a) Within a large-scale, decay-phase, topside F-layer depletion where "in situ" irregularities were reduced (compared with the depletion's topside wall), the radar's backscatter energy was also reduced (compared with the top-side wall). This result suggests the co-location of maximum radar returns with the upper regions of a depletion (its topside wall and above) and not with the depletion minimum or bottomside wall.

(b) The "in situ" measurements established field alignment of large scale depletions to distances at least as great as 163 km. This result supports the topside sounder data of Dyson and Benson (1968), the airglow observations of Weber et al., (1978), the recent radar measurements of Tsunoda (1980 a,b) and the assumption of depleted flux tubes in the theoretical considerations of Anderson and Haerendel (1979).

(c) Ion composition measurements within a topside
depletion showed little evidence of bottomside molecular
tracer ions (i.e., NO^+ and O_2^+). This result points to the
requirement for rapid bubble rise velocities and/or low
plasma densities ($N_e << 10^4$ cm^{-3}) within the hole if the
bottomside molecular ion composition is to be maintained as
bubbles drift upward through the F-region (Szuszczewicz,
1978). However, the measurements did reveal N^+ as a longer
lived tracer ion. This helped identify the lower altitude
source region to be on the bottomside F-layer gradient.

(d) Strong irregularities on the bottomside F-region
gradient showed O^+ following large scale density fluctuations
while the molecular ions NO^+ and O_2^+ were relatively constant.
Preliminary analysis of this result suggests chemical
equilibrium and eliminates neutral atmospheric turbulence as
a major source of the bottomside plasma irregularities.

(e) An estimate of bubble rise velocity was arrived at
by preliminary ion chemical analysis of composition within
the hole. The analysis suggests an upper limit of 600 m/sec
for the average vertical velocity of an 85% depleted domain
(85% on the topside, 100% at the F-peak) as it drifted
upward from its bottomside source region near 260 km to the
topside F-layer at 490 km. This upper limit is consistent
with the wide range in predicted values (Ossakow and Chaturvedi,
1978; Ossakow et al., 1979; Anderson and Haerendel, 1979).
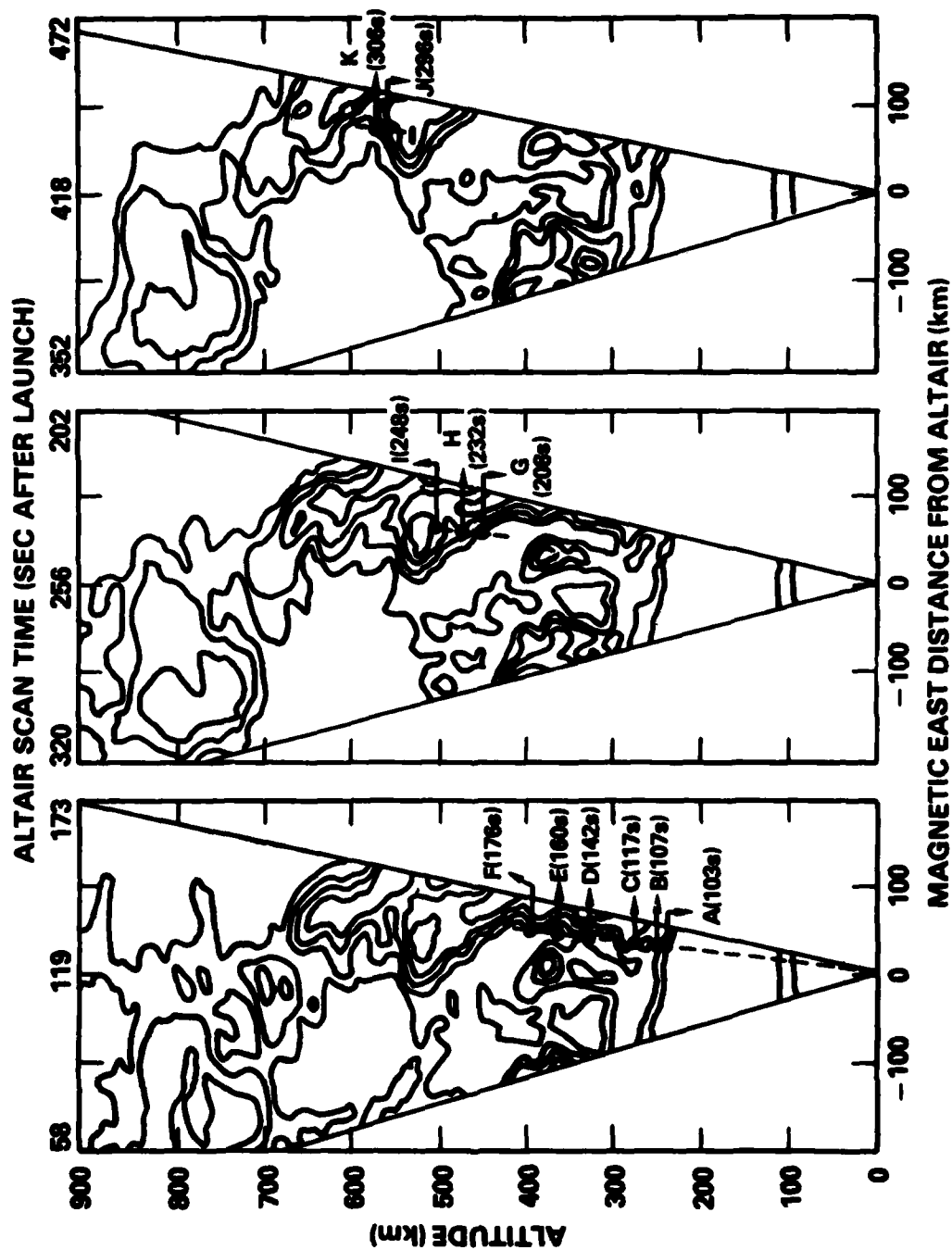
ACKNOWLEDGMENTS

Fig. 1 — Backscatter intensity contour maps (contours are in 10 dB increments) with superposition of the rocket trajectory. The times identified with observations "A" through "K" are included for a more complete representation of temporal correlation with the successive radar scans.
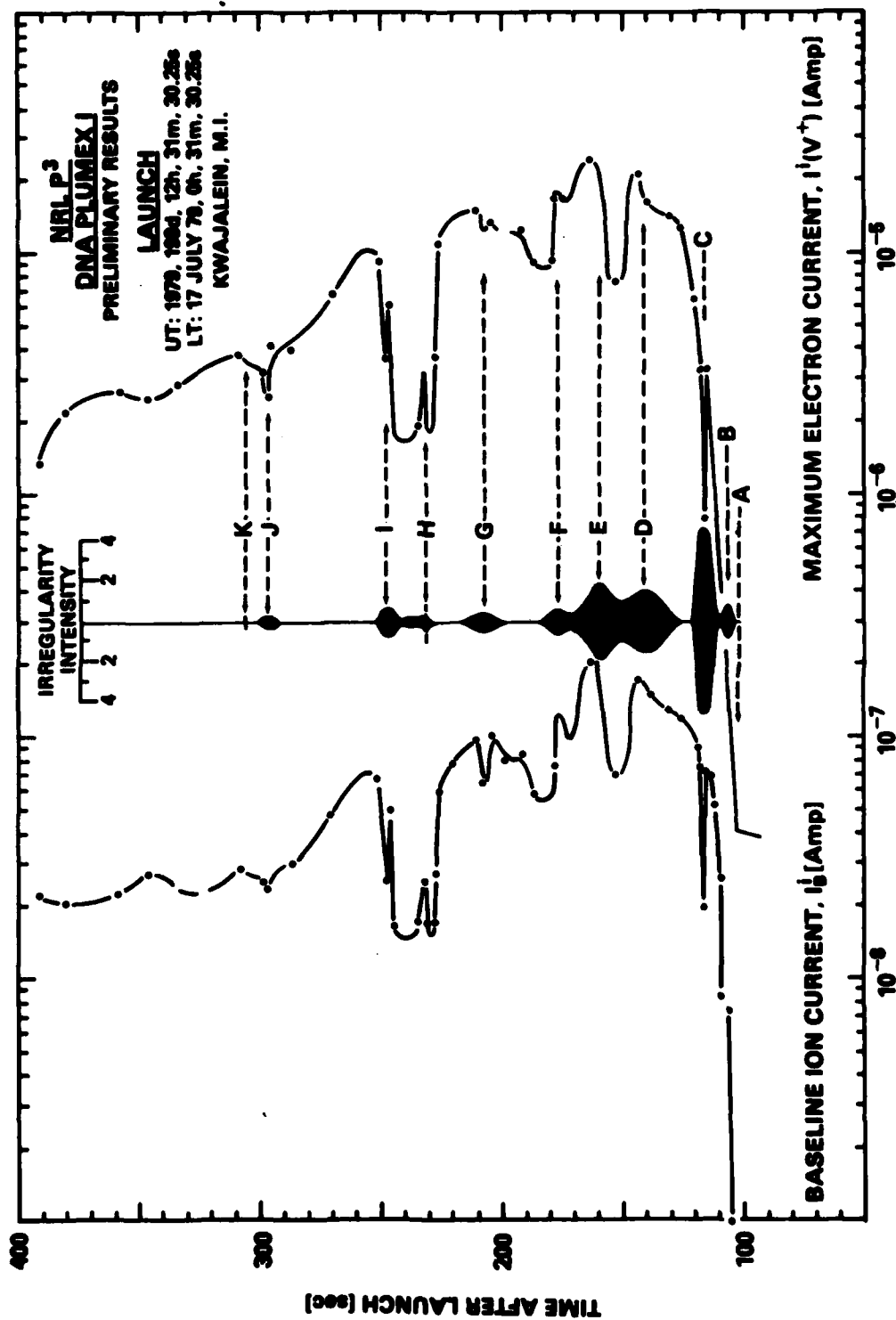
38

Fig. 2— Relative electron density profile as measured simultaneously by ion and electron saturation probe currents collected on the upleg trajectory. The "irregularity intensity" provides an approximate measure of smaller scale structure as scaled from analog strip chart records of probe current fluctuations.
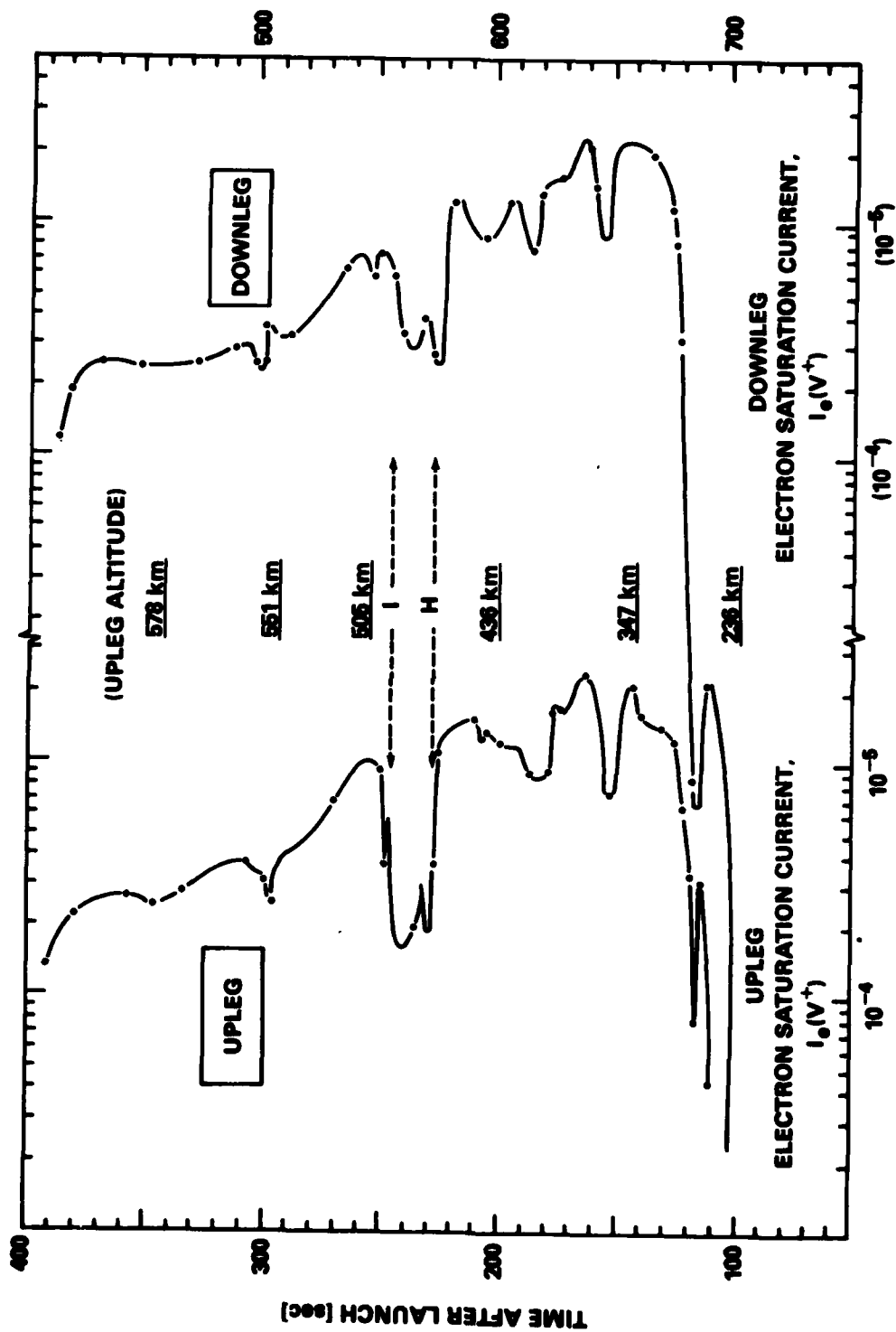
Fig. 3— Comparison of up- and downleg plasma profiles

40

REFERENCES

Anderson, D.N., and G. Haerendel, "The motion of depleted plasma regions in the equatorial ionosphere," J. Geophys. Res., 84, 4251, 1979.

Brinton, H.C., H. G. Mayr, and G. P. Newton, "Ion composition in the nighttime equatorial F-region: Implications for chemistry and dynamics" (abstract), Eos Trans. AGU, 56, 1038, 1975.

Dyson, P.L., and R.F. Benson, "Topside sounder observations of equatorial bubbles," Geophys. Res. Lett. 5, 795, 1978.

Kelly, M.C., G. Haerendel, H. Kappler, A. Valenzuela, B.B. Balsley, D.A. Carter, W.L. Ecklund, C.W. Carson, B. Hausler, and R. Torbert, "Evidence for a Rayleigh-Taylor type instability and upwelling of depleted density regions during equatorial spread F," Geophys. Res. Lett., 3, 448, 1976.

McClure, J.P., W.B. Hanson, and J.H. Hoffman, "Plasma bubbles and irregularities in the equatorial ionosphere," J. Geophys. Res., 82, 2650, 1977.

Morse, F. A., B.C. Edgar, H.C. Koons, C.J. Rice, W.J. Heikkila, J.H. Hoffman, B.A. Tinsley, J.D. Winningham, A.B. Christensen, R.F. Woodman, J. Pomalaza, and N.R. Teizeira, "Equion, and equatorial ionospheric irregularity experiment," J. Geophys. Res., 82, 578, 1977.

Ossakow, S. L., and P.K. Chaturvedi, "Morphological studies of rising equatorial spread-F bubbles," J. Geophys. Res., 83, 2084, 1978.

Ossakow, S.L., S.T. Zalesak, B.E. McDonald, and P.K. Chaturvedi, "Nonlinear equatorial spread F: Dependence on altitude of the F peak and bottomside background electron density scale length," J.Geophys. Res. 84, 17, 1979.

Scannapieco, A.J., and S.L. Ossakow, "Nonlinear equatorial spread F," Geophys. Res. Lett., 3, 451, 1976.

Szuszczewicz, E.P. and J.C. Holmes, "Observations of electron temperature gradients in mid-latitude E_s layers," J. Geophys. Res., 82, 5073, 1977.

Szuszczewicz, E.P., "Ionospheric holes and equatorial spread-F: Chemistry and transport," J. Geophys. Res. 83, 2665, 1978.

Szuszczewicz, E.P., and P.Z. Takacs, "Magnetosheath effects
    on cylindrical Langmuir probes," Phys. Fluids 22,
    2424, 1979.

Tsunoda, R.T., M.J. Baron, J. Owen and D.M. Towle, "Altair:
    An Incoherent scatter radar for equatorial spread-
    F studies," Radio Sci., 14, in press, 1979.

Tsunoda, R.T., "On the spatial relationship of 1-m equatorial
    spread-F irregularities and plasma bubbles," J.
    Geophys. Res. 85, (in press, 1980a).

Tsunoda, R.T., "Magnetic-field-aligned characteristics of
    plasma bubbles in the nighttime equatorial ionosphere,"
    J. Atmos. Terr. Phys. (submitted, January 1980).

Weber, E.J., J. Buchau, R.H. Eather, and S.B. Mende, "North-
    south aligned equatorial airglow depletions," J. Geophys.
    Res., 83, 712, 1978.

Woodman, R.F., and C. LaHoz, "Radar observations of F region
    equatorial irregularities," J. Geophys. Res., 81,
    5447, 1976.

NRL Memorandum Report 4289

Equatorial Spread F:
"In Situ" Measurements of Electron Density
Temperature and Density Fluctuation Power Spectra

E.P. SZUSZCZEWICZ AND J.C. HOLMES

Ionospheric Diagnostics Section
Space Science Division

August 25, 1980

NAVAL RESEARCH LABORATORY
Washington, D.C.

REPORT DOCUMENTATION PAGE		READ INSTRUCTIONS BEFORE COMPLETING FORM
1. REPORT NUMBER NRL Memorandum Report 4289	2. GOVT ACCESSION NO.	3. RECIPIENT'S CATALOG NUMBER
4. TITLE (and Subtitle) EQUATORIAL SPREAD F: "IN SITU" MEASUREMENTS OF ELECTRON DENSITY TEMPERATURE AND DENSITY FLUCTUATION POWER SPECTRA		5. TYPE OF REPORT & PERIOD COVERED Interim report on a continuing DNA problem.
		6. PERFORMING ORG. REPORT NUMBER
7. AUTHOR(s) E.P. Szuszczewicz and J.C. Holmes		8. CONTRACT OR GRANT NUMBER(s)
9. PERFORMING ORGANIZATION NAME AND ADDRESS Naval Research Laboratory Washington, D.C. 20375		10. PROGRAM ELEMENT, PROJECT, TASK AREA & WORK UNIT NUMBERS 62710H; 71-0950-0-0
11. CONTROLLING OFFICE NAME AND ADDRESS Defense Nuclear Agency Washington, D.C. 20305		12. REPORT DATE August 25, 1980
		13. NUMBER OF PAGES 35
14. MONITORING AGENCY NAME & ADDRESS(if different from Controlling Office)		15. SECURITY CLASS. (of this report) UNCLASSIFIED
		15a. DECLASSIFICATION/DOWNGRADING SCHEDULE

16. DISTRIBUTION STATEMENT (of this Report)

Approved for public release; distribution unlimited.

17. DISTRIBUTION STATEMENT (of the abstract entered in Block 20, if different from Report)

19. KEY WORDS (Continue on reverse side if necessary and identify by block number)

Absolute density
Temperature
Density fluctuation power spectra
In Situ irregularities

20. ABSTRACT (Continue on reverse side if necessary and identify by block number)

The NRL pulsed plasma probe experiment was successfully flown on each of the two PLUMEX rockets during July 1979. The experiment provided direct measurements of absolute density N_e, temperature T_e and density fluctuation power spectra with a maximum Nyquist frequency of 1 KHz (1 meter resolution at a 1 km/sec rocket velocity). In the first operation, a number of major depletions ($\Delta N_e/N_e^0 \lesssim 90\%$) were distributed throughout the F-region, from its bottomside gradient centered near 260 km,

(Continues)

DD FORM 1473 EDITION OF 1 NOV 65 IS OBSOLETE
1 JAN 73
S/N 0102-LF-014-6601

44

20. Abstract (Continued)

through the F-peak, to a topside altitude of 500 km. The F-peak was at 375 km, with $N_e^{max} = 1.3 (10^6)$ cm^{-3} ($\pm$ 10%). The electron energy distribution was characterized by $T_e = 1350$ ($\pm$ 250)$^{\circ}$K with no obvious signatures of energy redistribution in and around the depletions. The most intense "in situ" irregularities occurred on the bottomside ledge where gradient scale lengths were found to vary between 2 and 25 km. The power spectral density in this region of intense irregularities on the bottomside was dominated by a $k^{-2.5}$ power law over the intermediate wavelength domain $k = 2\pi/1$ km to $k = 2\pi/2.5$ m. This result supports the role of the collisional Rayleigh-Taylor instability in generating intermediate wavelength irregularities during the occurrence of equatorial spread-F.

PART III
CONTENTS

EQUATORIAL SPREAD F:
"IN SITU" MEASUREMENTS OF ELECTRON DENSITY
TEMPERATURE AND DENSITY FLUCTUATION POWER SPECTRA

I. INTRODUCTION

The DNA/PLUMEX rocket payloads launched into the equatorial
ionosphere during the July 1979 campaign carried a plasma
diagnostics complement that included a quadrupole ion mass
spectrometer, a pair of pulsed plasma probes, vector electric
field sensors and a four-frequency beacon. The pair of
pulsed plasma probes not only provided simultaneous measure-
ments of electron density N_e, temperature T_e, and density
fluctuation power spectra $P_n(k)$, but also provided the
capability for a running measurement of relative variations
in mean ion mass $<M_i>$.

The measurements of N_e and T_e form the basic information
on the laminar condition of the ionosphere, allowing for the
determination of the ionospheric plasma response to varying
geophysical conditions (solar and magnetic activity, winds,
gravity waves, etc.) and the detection of triggering mecha-
nisms (e.g., steep density gradients in N_e) for ionospheric
irregularities.

The measurements of $\delta N_e (\rightarrow P_n(k))$ yield important test
information for signal channel models as well as candidate
instability mechanisms (e.g., collisional drift modes, $\bar{E} \times \bar{B}$
and Rayleigh-Taylor) which might be active in the ionospheric
plasma.

In this paper we describe the experimental technique,
payload configuration, launch scenerios and present additional
experimental results which complement companion papers[1,2].

II. TECHNICAL OVERVIEW

Introduction. The pulsed plasma probe technique (P^3 is
the designated acronym) is a unique diagnostic tool capable
of high spatial and temporal resolution of plasma parameters.
The instrument is a Langmuir-type probe using a special
electronic procedure for generating the current-voltage
characteristic[3,4]. The result is greatly improved reliability
and expanded versatility in Langmuir probe measurements. As
a diagnostic tool, the P^3 technique reduces commonly found
distortions in derived electron densities and energy distribution
functions. A unique feature of the technique is its ability
to measure simultaneously the electron temperature, density,
and the density fluctuation power spectrum. Successful
applications of the P^3 technique include not only rocket but
also satellite [5,6] and laboratory beam-plasma studies[7] of
turbulent charged-particle environments.

Figure 1 shows two types of probe operation. Figure
1(A) depicts a linear sawtooth sweep voltage which represents
the conventional approach to Langmuir probe operation wherein
some form of continuous voltage sweep is applied between
voltage limits V_- and V_+. Fig. 1(B) shows the pulse-modulated
sweep which has been utilized with P^3. The voltage pulses
which follow the sawtooth envelope generate the probe's
current-voltage characteristic. During the interpulse
period, at constant voltage V_B, the collected probe current
I_B provides a direct measure of variations in the probe-
plasma system. The pulse duty-cycle is short so that the

probe rests at its baseline potential V_B for a period much longer than the pulse width. Fig. 2 shows pulse and baseline durations identified as τ_{on} and τ_B, respectively. So that sweep voltage transients will not affect the value of probe current, the probe current is sampled at the termination of subinterval τ_i within the sweep pulse and at the center of the baseline interval τ_B.

With τ_{on} much shorter than either τ_B or the time constant of the probe surface contamination layer[4], the pulse procedure will maintain the surface condition and associated voltage drop at a more nearly constant level than when using a continuous, slowly-varying sweep voltage. The resulting current-voltage characteristic can then be unfolded from the plasma density fluctuations (δI_B) so that the electron temperature and density are determined uniquely. In addition, the I_B-values provide the raw data from which density fluctuation power spectra are determined.

Payload configuration and P^3 characteristics. A pair of pulsed probes were diametrically extended from the forward end of the rocket payload (Fig. 3). The sensing elements constructed from tungsten wire, were isolated from their extension booms by coaxial guard electrodes driven at the same potential as the probes themselves. One of the probes, defined as the I-probe, operated with $V_B \sim -1v$, yielding net ion baseline current I_B^i. The other probe, defined as the E-probe, operated with $V_B \sim +2v$, yielding net electron baseline current I_B^e. Both probes generated

complete current-voltage characteristics in $\tau_s \sim 400$ msec, yielding absolute values of N_e and T_e at an approximate 2.5 Hz rate. Maximum I_B sampling occurred at 2048 Hz, resulting in 0.5 meter spatial resolution for relative electron density fluctuations at a vehicle velocity of 1 km/sec.

Probe electrometers were set to operate over a dynamic range extending from $4(10^{-10})$ to 2.5 (10^{-4}) amperes, with automatic switching over 8 ranges maintaining 9 bit accuracy for all anticipated ionospheric conditions. The automatic ranging is best illustrated in Figure 4, an actual in-flight analog record of telemetry channel outputs for the probe currents and applied voltages, the roll magnetometer for magnetic aspect determinations, and pitch, yaw and roll monitors on the ACS jets. The data sample presented in Figure 4 was collected when the payload was 55 seconds into flight while the probe electrometers were being driven through a load resistor for calibration. The probes' operation alternated between a fixed-bias mode and a pulsed-sweep mode, with absolute currents determined by a simple algorithm which coupled the switching 0-5 v TM signal on PCM channel 26-1 with the sweep current range monitor on channel 27-1. The record format in Fig. 4 helped provide field-estimates of density profiles without distortions of magnetic aspect sensitivities and a.titude control jets.

III. RESULTS

Density profiles and irregularity structures. By 9 P.M. (LT) on the night of the first rocket launch (PLUMEX I) the bottomside of the F-region had risen to an approximate

altitude of 400 km. The F-region then began a downward
drift with a simultaneous onset of spread-F. The downward
drifting and spread-F conditions continued, and when the
bottomside F-layer had descended to an altitude below 300
km, the rocket was launched (12:31:30 UT on day 198; 00:31:30,
17 July 1979, LT).

Figure 5 displays the upleg measurements of relative
electron density as presented by correlated ion- (I_B^i) and
electron- saturation $I_e^i(V^+)$ currents. The ordinate has a
linear scale for time-after-launch with altitude super-
imposed at 50 second increments. Because ion and electron
saturation currents have significantly different sensitivities
to velocity, sheath and magnetic field effects[8], variations
in I_B^i and $I_e^i(V^+)$ not mutually corroborated were attributed
to the various aspect sensitivities and excluded from Figure
5. This approach facilitated analysis, reduced computer
time, and established credibility in the interpretation of
the curves as relative electron density profiles.

The results in Figure 5 show that a number of major
depletions ($\Delta N_e/N_e^o \lesssim 0.9$) were distributed throughout the F-
region. Each of the large scale depletions (identified
alphabetically) has its own distribution of irregularities,
illustrated in Fig. 6 by the expanded view of regions C, D,
H and I. It is clear that "C" is not a single narrow bite-
out but a collection of rather large irregular structures

extending over a total altitude domain of about 12 km.
(Vehicle velocity in region C was 2.4 km/sec.) To develop a
quantitative view of irregularity fluctuations observed in
the F-region, continuous linear detrends were executed
throughout the entire upleg trajectory. The variations
about those linear detrends were then plotted in Figure 5 as
"Irregularity Intensity", with a maximum relative scale of
$\pm$ 4. A fluctuation as great as $\pm$ 4 approximately represents
a $\pm$ 80% fluctuation about the linear detrend. (Correlation
of these results with macroscale gradients and Altair back-
scatter contours are discussed in a companion paper[1].

Absolute density and temperature. Absolute values of
electron density and temperature were determined by conven-
tional analyses of Langmuir probe characteristics[9] with
appropriate care to eliminate perturbing effects of surface
contamination[4], density fluctuations[3,10] and magnetic field
effects[8]. Analysis of approximately 25 characteristics were
executed over the F-layer from 340-560 km. In each case a
conversion coefficient $a \equiv N_e$ [cm^{-3}]$/I_e(V^+)$ was determined
so that the $I_e(V^+)$ profile in Figure 5 could be directly
scaled to absolute electron densities. This procedure
yielded $a = (5.5 \pm 0.5) \, 10^{10}$ electrons cm^{-3}A^{-1}.

The upleg profile has been reconstructed in Figure 7
with relative and absolute electron density plotted as a
function of altitude. The result shows the F-peak at 375
km, with a maximum density of 1.3 (10^6)cm^{-3} ($\pm$ 10%).

Analysis of the retarding-field region of the same set of current-voltage characteristics yielded $T_e = (1350 \pm 250)^\circ K$, with no obvious signatures of electron energy redistribution in and around the depletions.

Intermediate wavelength power spectra. The pulsed probe data provided an excellent opportunity for comparison with the numerical simulations[11] of the collisional Rayleigh-Taylor (R-T) instability at intermediate wavelengths. Attention is focused on the bottomside F-layer gradient and region C, which is believed representative of the mid-phase development of the R-T process[1]. Typically, computer simulations employ several values for the zero-order gradient scale length

$$L = \left(\frac{1}{N_e^o} \frac{dN_e^o}{dy} \right)^{-1}$$

and initialize the code with some two-dimensional perturbation superimposed. In the work of Keskinen, et al.[11] L was selected at 5, 10 and 15 km and the perturbation took the form [12]

$$\frac{\delta N_e(x,y,t=0)}{N_e^o} = (10^{-4}) \, Sin \, (k_y \, y) \, Cos \, (k_x \, x) + 2(10^{-6}) \, Sin \, (2k_y \, y)$$

with k_x and k_y being the horizontal and vertical wavenumbers, respectively. Both k_x and k_y were set equal to $2\pi/960$ m in the simulation. In addition, the computation assumed that L was centered at 300 km.

Under actual conditions encountered in PLUMEX I (Fig 7), the bottomside F-layer gradient extended from 240 to 290 km. The question of gradient scale length can be studied in Figure 8 where it is shown that the bottomside gradient (encompassed in the 105-125 sec time frame) is not characterized by a single value of L. In region "C" ($114s \lesssim t \lesssim 122s$) L is seen to vary between 2 and 10 km, whereas adjacent domains ($110s \leq t \leq 113s$ and $122s \leq t < 126s$) can be characterized by L = 25 km. We would suggest that the adjacent domains are representative of the zero-order gradient scale length and that L = 25 km would be a more appropriate value in the numerical simulation.

In any event, computer simulations[11] with L = 5, 10 and 15 km showed that linearly unstable modes saturate by non-linear generation of vertical modes. The results yield one-dimensional power laws (horizontal and vertical) that vary with a spectral index ($\equiv$ n in $P_{N_e} \propto k^{-n}$) between 2.0 and 2.5. To explore this result within the context of region "C", power spectral analyses were conducted over sliding intervals of 2.4 km. The results, presented in Figure 9, show that the dominant behavior is $k^{-2.5}$ over the range k = $2\pi/1$km to k = $2\pi/25$m. The $k^{-1.85}$ behavior at t = 116.001 sec is a result of the very sharp density gradient (see region "C" Fig. 6) encompassed by the domain of the spectral analysis.

In general we would conclude that our results support the numerical simulations of Keskinen, et al.[11]. We do

point out however that a spectral index variation from 2 to 2.5 is a rather broad domain. Further testing of this support can be achieved with an L = 25 km simulation and a downward drifting F-layer model that is more in keeping with the actual experimental conditions. The F-layer time-history can be important since unstable modes appear to require times in excess of 4,000 seconds to saturate...a time during which the F-layer encountered in PLUMEX I drifted downward in excess of 40 km.

IV. SUMMARY

In each of the two rocket operations (PLUMEX I & II) conducted at the Kwajalein Atoll during July 1979, the NRL pulsed plasma probe performed flawlessly. General results concerning coordinated rocket and radar measurements of small and large scale irregularities have been discussed in companion papers[1,2]. Complementary results developed here include:

(a) In PLUMEX I a number of major depletions ($\Delta N_e/N_e^o \lesssim$ 90%) were distributed throughout the F-region, from the bottom-side gradient centered near 260 km, through the F-peak, to a topside altitude of 500 km. The most intense "in situ" irregularities occurred on the bottomside ledge where gradient scale lengths were found to vary between 2 and 25 km. The power spectral density in this region of intense irregularities on the bottomside was dominated by a $k^{-2.5}$ power law over the intermediate wavelength domain $k = 2\pi/1\text{km}$ to $k = 2\pi/2.5\text{m}$. The experimental conditions were reasonably matched to the

numerical simulations of Keskinen et al.[11], and a comparison of the two resulted in general agreement.

(b) In PLUMEX I, the F-peak was at 375 km, with $N_e^{max} =$ 1.3 (10^6) cm^{-3} ($\pm$ 10%). The electron energy distribution was characterized by $T_e = (1350 \pm 250)^\circ K$ with no obvious signatures of energy redistribution in and around the depletions.

REFERENCES

1. Szuszczewicz, E.P., R.T. Tsunoda, R. Narcisi and J.C. Holmes, "PLUMEX I: Coincident radar and rocket observations of equatorial spread-F," DNA Report ,1980; also published in Geophys. Res. Lett. (in press,July 1980).

2. Szuszczewicz, E.P., R.T. Tsunoda, R. Narcisi and J.C. Holmes, "PLUMEX II: Coincident radar and rocket observations of equatorial spread-F," DNA Report, 1980; also published as NRL Memorandum Report (in press 1980).

3. Holmes, J.C. and E.P. Szuszczewicz, "A versatile plasma probe," Rev. Sci. Instr. 46, 592 (1975).

4. Szuszczewicz, E.P. and J.C. Holmes, "Surface contamination of active electrodes in plasmas: Distortion of conventional Langmuir probe measurements," J. Appl. Phys. 46, 5134 (1975).

5. Szuszczewicz, E.P., J.C. Holmes and D.N. Walker, "On the probing of ion and electron irregularity spectra." EOS 60, 339 (April 1980).

6. Singh, M., E.P. Szuszczewicz and J.C. Holmes, "High resolution measurements of equatorial F-region irregularities," EOS 61, 314 (April 1980).

7. Szuszczewicz, E.P., J.C. Holmes, and D.N. Walker, "Plasma diffusion in a space-simulation beam-plasma-discharge", Geophys. Res. Lett. 6, No. 3 (1979).

8. Szuszczewicz, E.P. and P.Z. Takacs, "Magnetosheath effects on cylindrical Langmuir probes," Phys. Fluids 22, 2424 (1979).

9. Chen, F.F., "Electrical probes," in Plasma Diagnostic Techniques, edited by R.H. Huddlestone and S.L. Leonard (Academic, New York, 1965), p. 113.

10. Szuszczewicz, E.P. and J.C. Holmes, "Observations of electron temperature gradients in mid-latitude E_s layers," J. Geophys. Res., <u>82</u>, 5073, 1977.

11. Keskinen, M.J., S.L. Ossakow and P. K. Chaturvedi, "Preliminary report on numerical simulations of intermediate wavelength collisional Rayleigh-Taylor instability in equatorial spread-F," J. Geophys. Res. <u>85</u>, 1775 (1980).

12. Chaturvedi, P.K., and S.L. Ossakow, "Nonlinear theory of the collisional Rayleigh-Taylor instability in equatorial spread-F," Geophys. Res. Lett. <u>4</u>, 558 (1977).
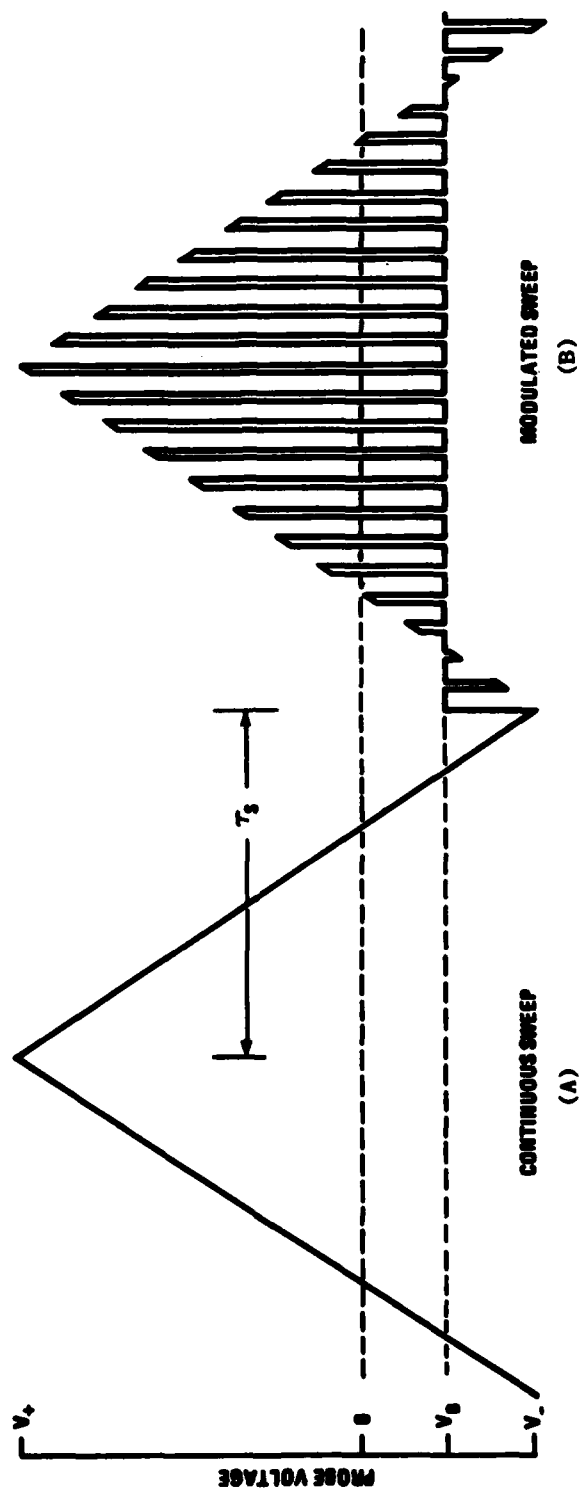
Fig. 1 — Continuous and pulsed modes of probe operation. (A) represents the conventional approach, while (B) shows the modulated sweep utilized in the P³ technique.

SWEEP PULSE

τ_B

τ_{ON}
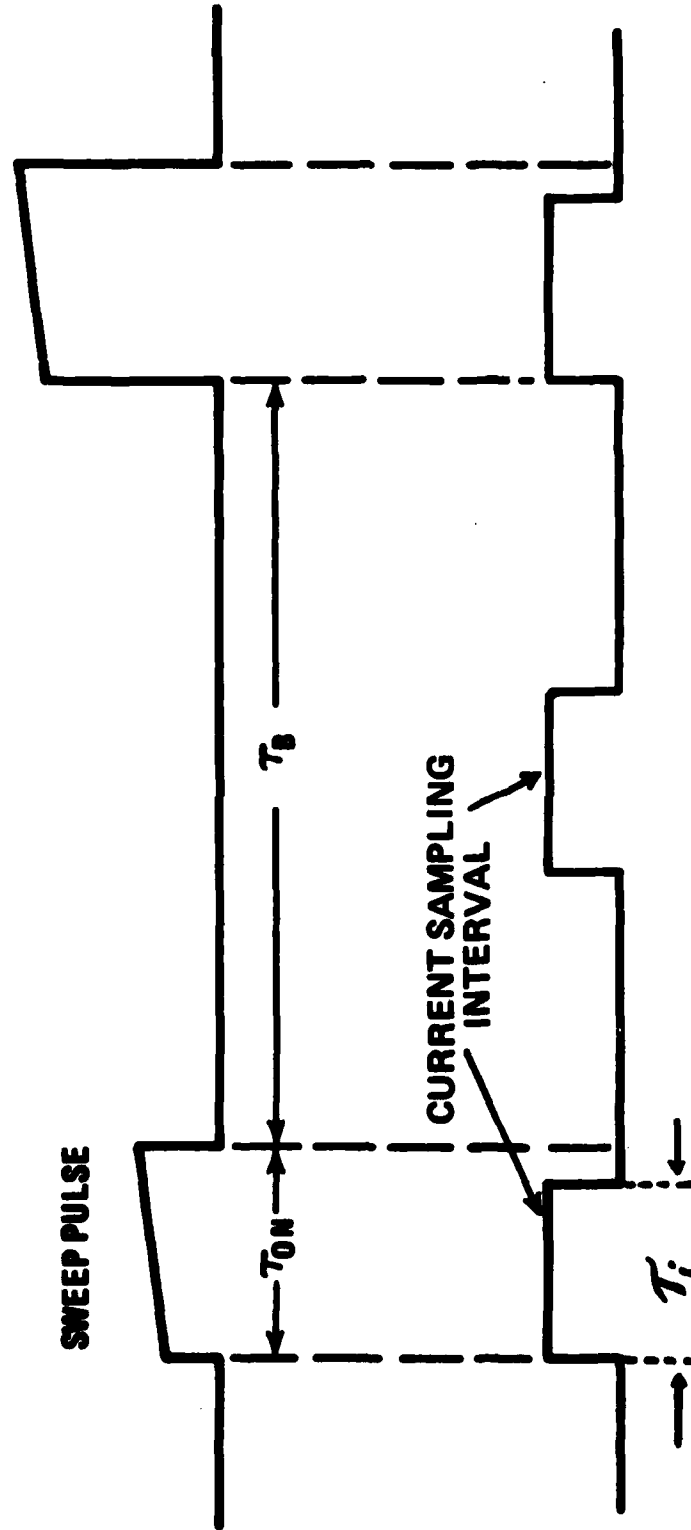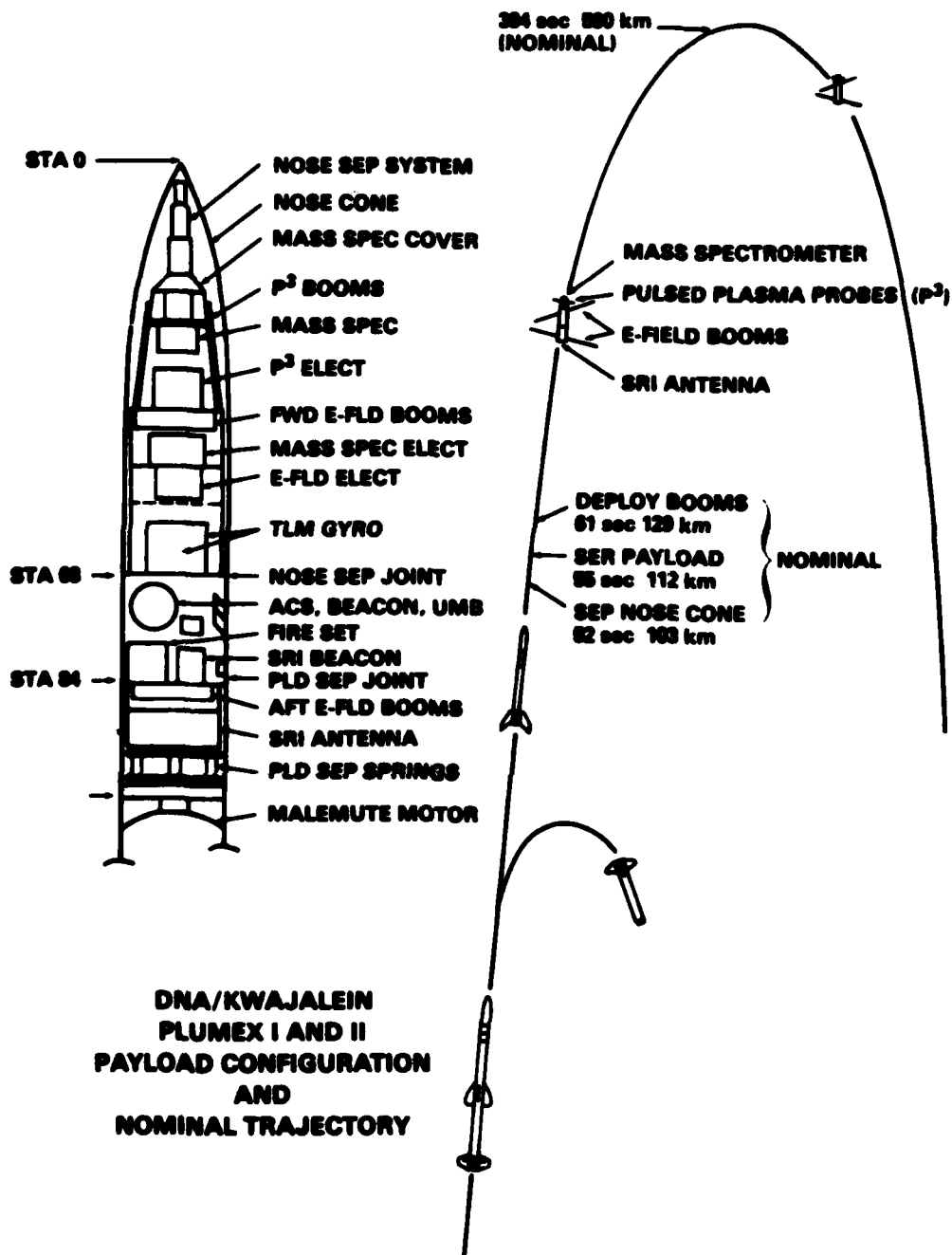
CURRENT SAMPLING
INTERVAL

τ_i

Fig. 2 — The sweep pulses (Fig. 1) shown on an expanded scale to illustrate the probe-current sampling intervals

Fig. 3 — PLUMEX payload configuration and nominal trajectory.
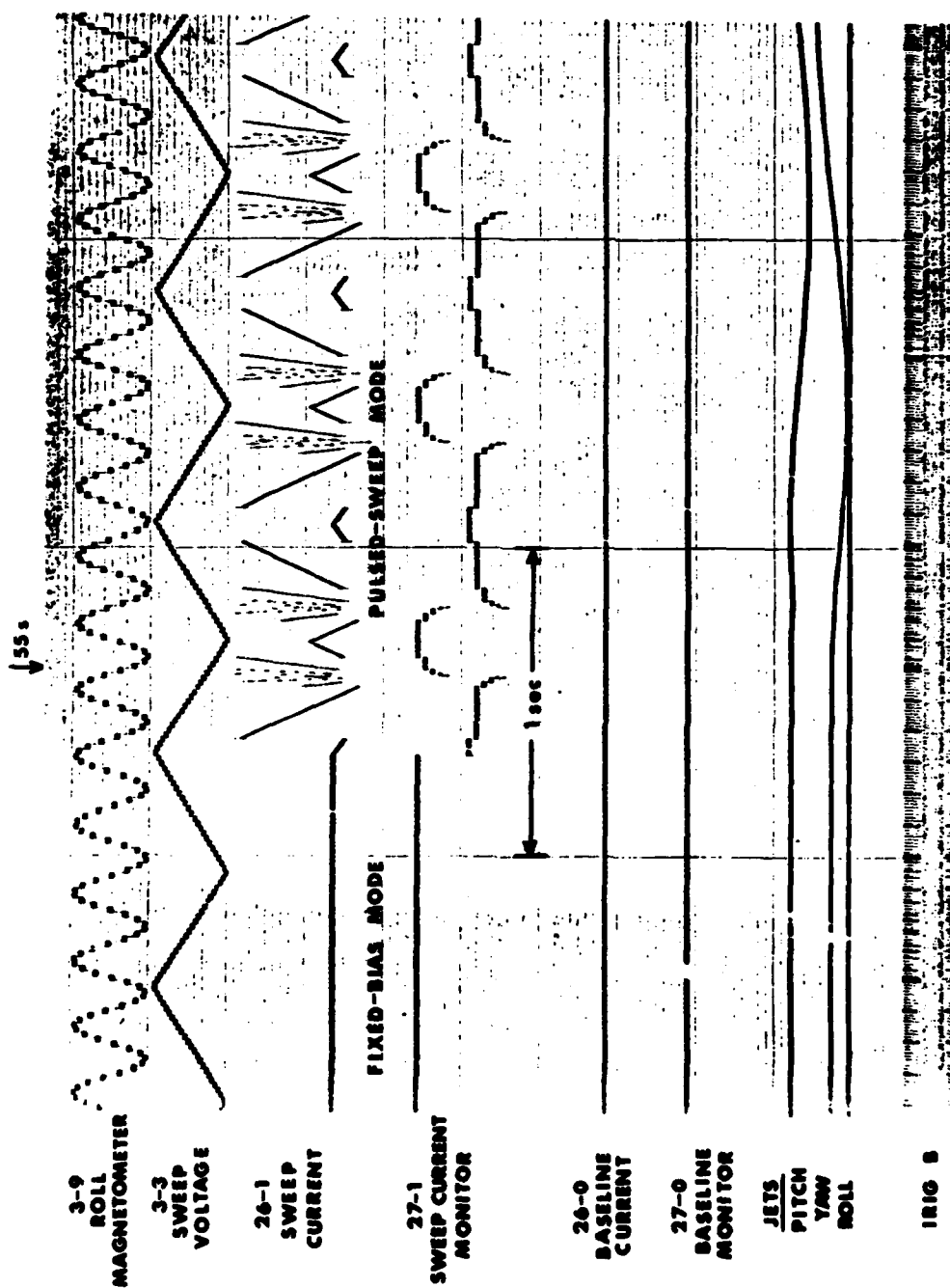(This figure has been adapted from a Sandia report.)

Fig. 4 — Analog record of PLUMEX I telemetry channels (3-9, 3-3, etc.) illustrating pulsed-plasma-probe outputs and relevant vehicle information (roll-magnetometer, attitude control jets and IRIG B timing). The probe electrometers (26-1) cover six decades of current in 8 automatic-switching ranges (26-1 shows automatic ranging, while 27-1 identifies each range through a simple algorithm). 9 bit accuracy is maintained throughout.
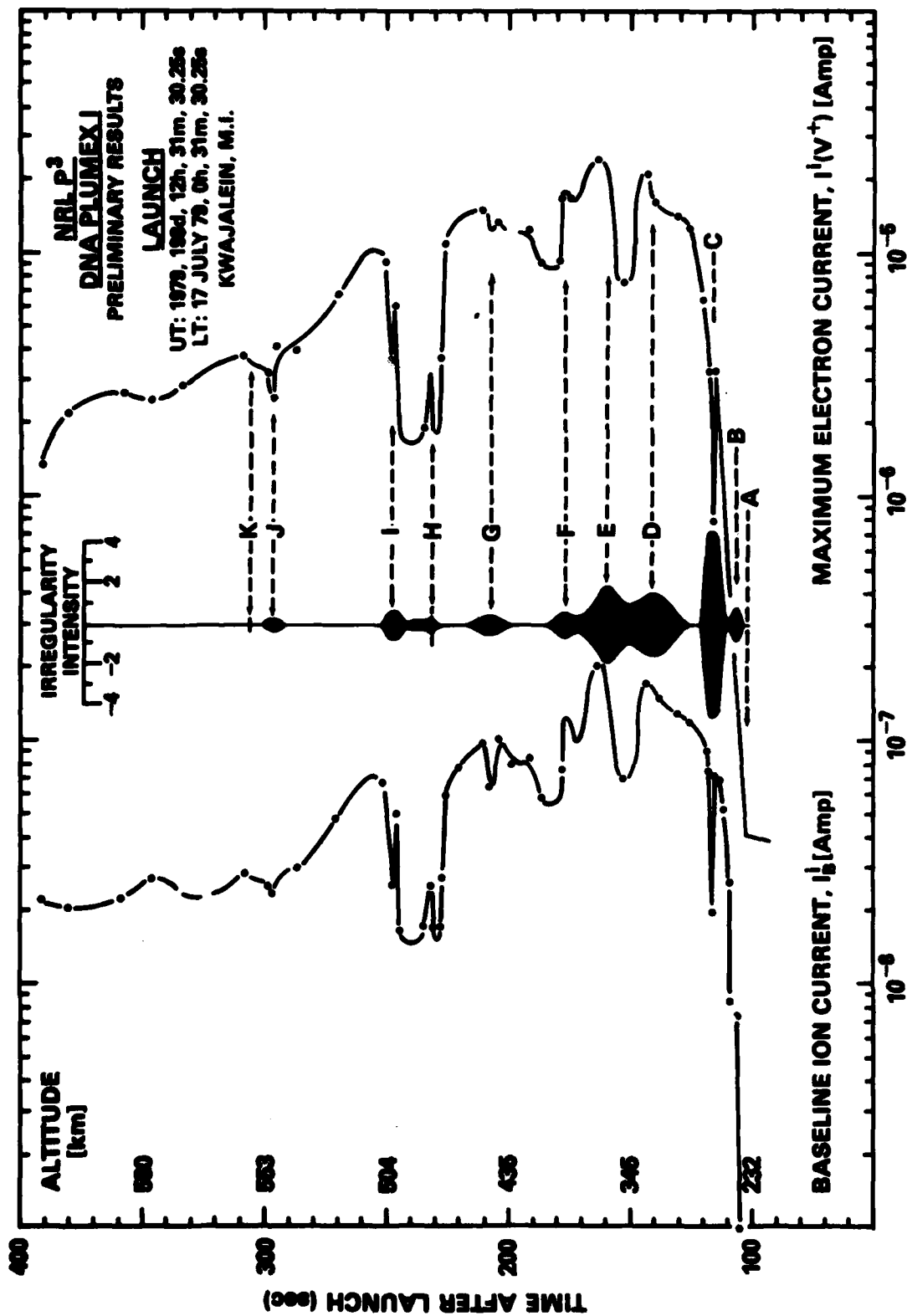
Fig. 5 — Relative electron density profile of macroscale features as measured simultaneously by ion and electron saturation probe currents collected on the upleg trajectory of PLUMEX I. The "irregularity intensity" provides a measure of smaller scale structure with a ± 4 intensity approximately equal to ± 80% fluctuations about a linear detrend.
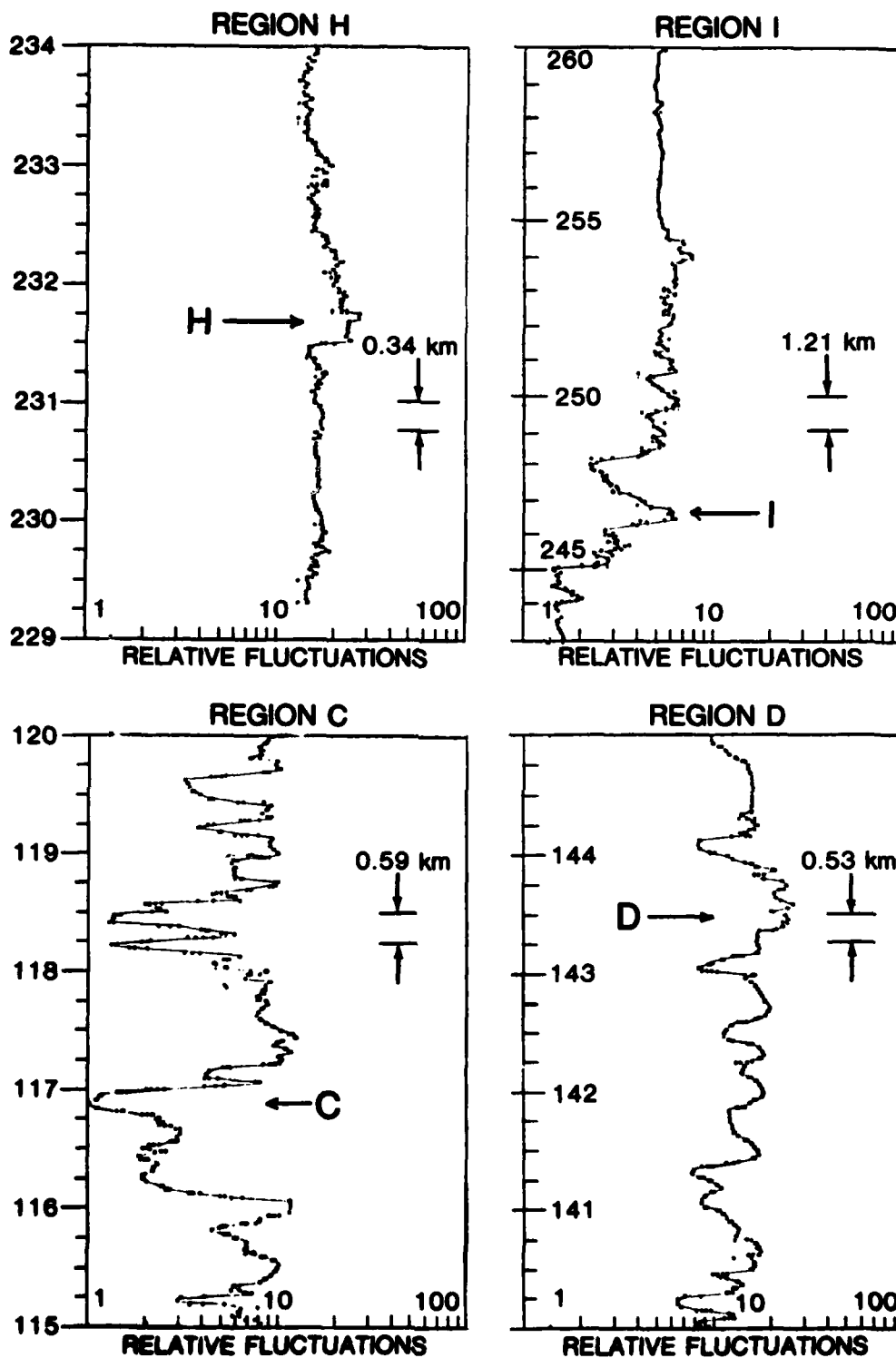
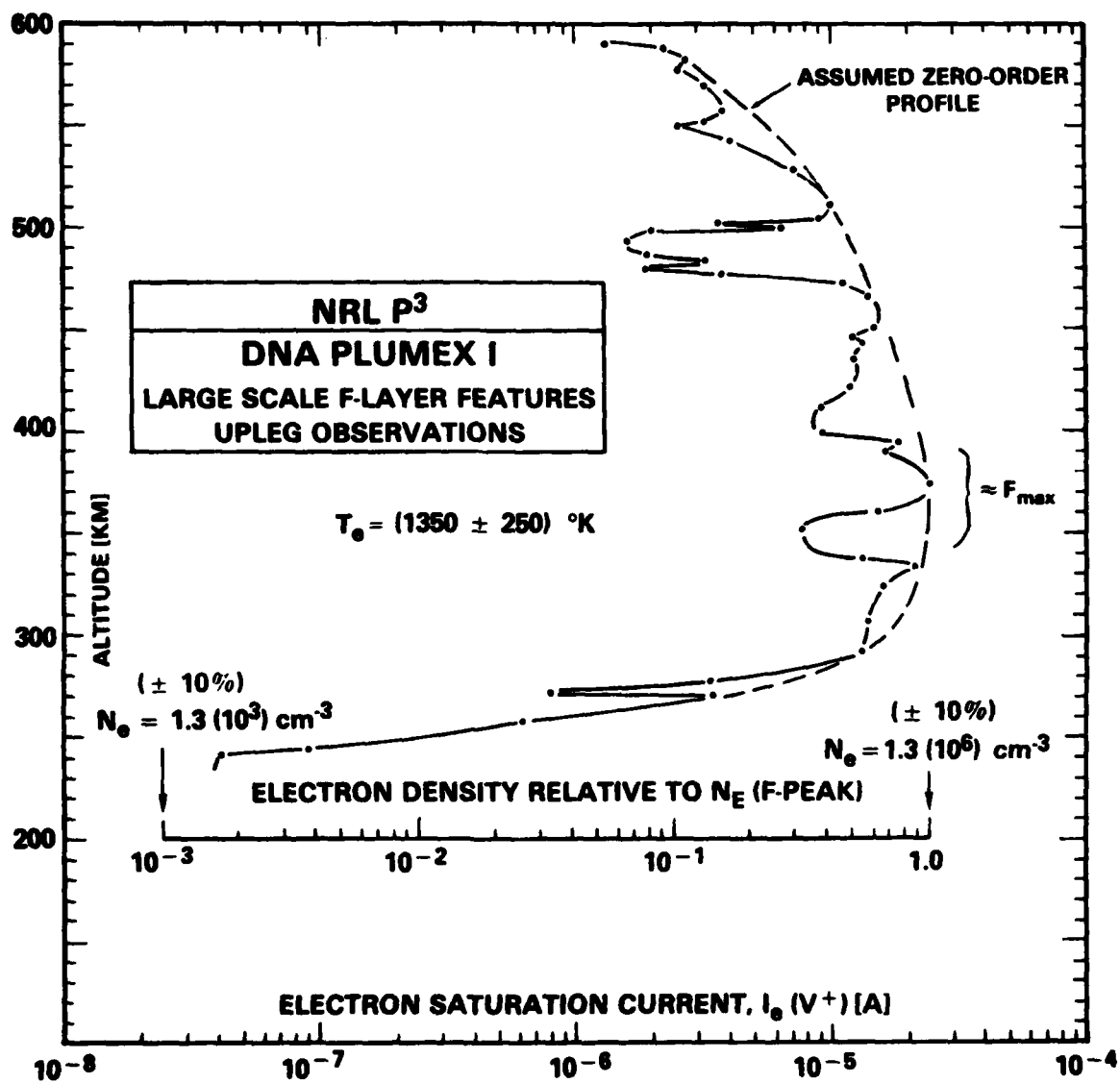**Fig. 6 — Expanded views of density fluctuations observed in regions C,D,H and I of Fig. 5**

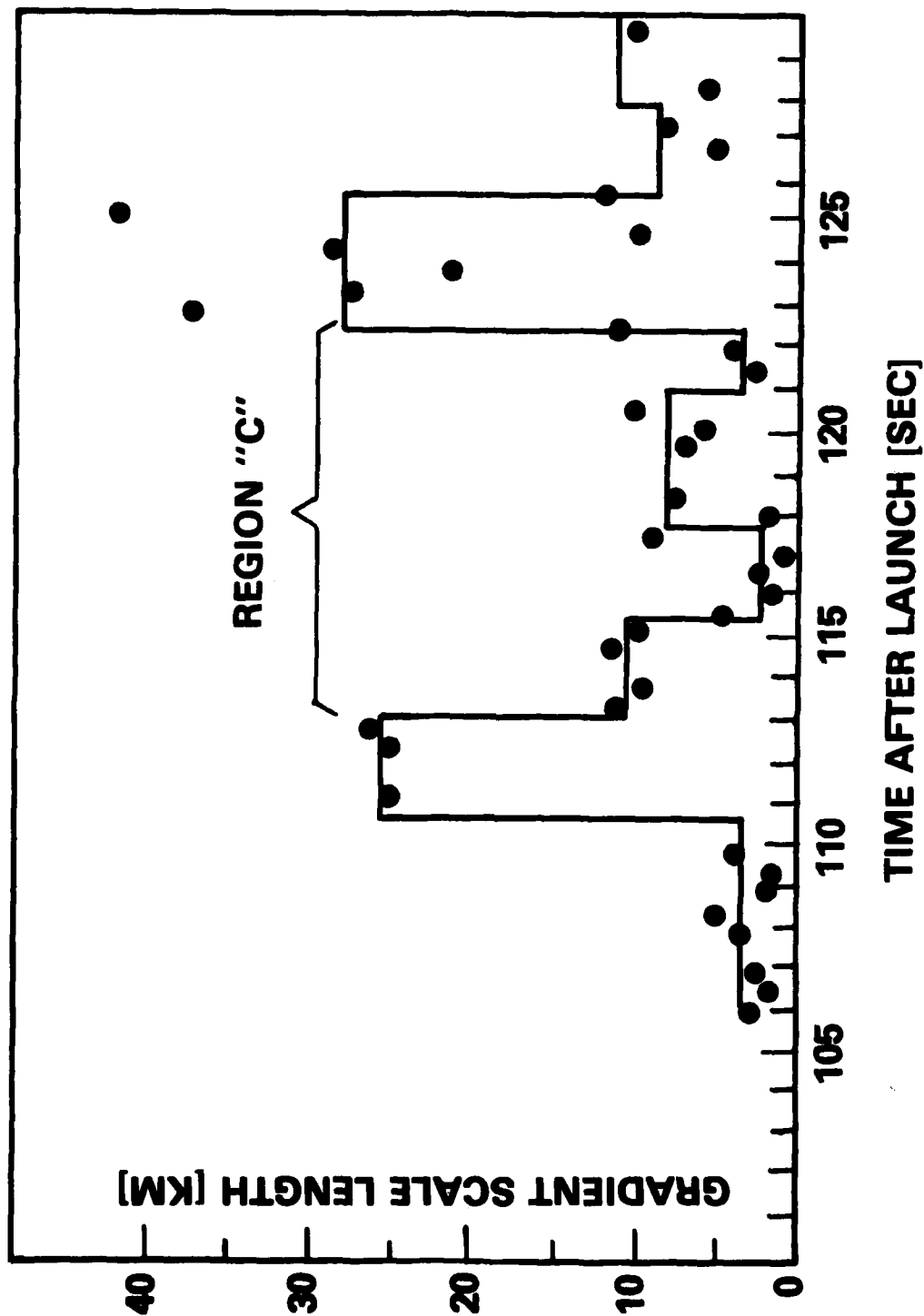Fig. 7 — Relative and absolute profile of electron density (PLUMEX I upleg)

Fig. 8 — Gradient scale lengths $\left(L = \left[\dfrac{1}{N_e^o} \dfrac{dN_e^o}{dy} \right]^{-1} \right)$ on the bottomside gradient of the F-region layer shown in Figs. 5 and 6
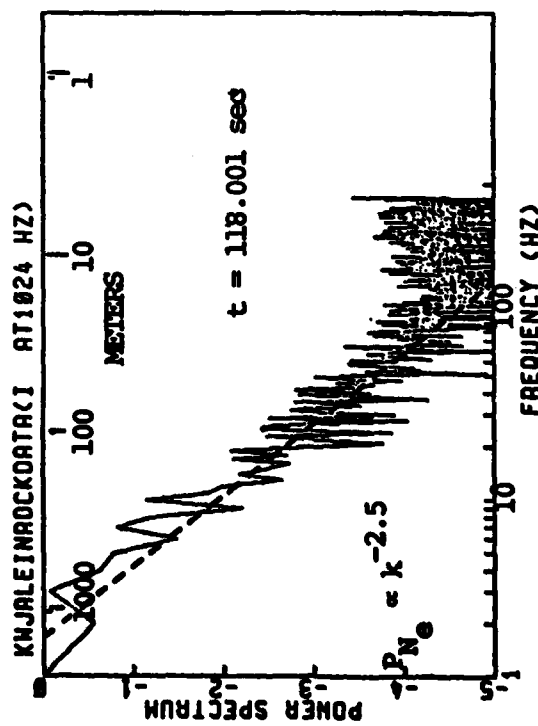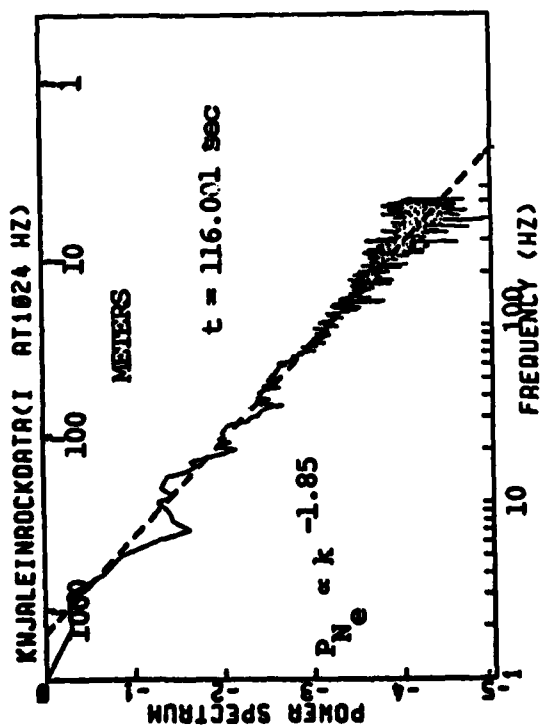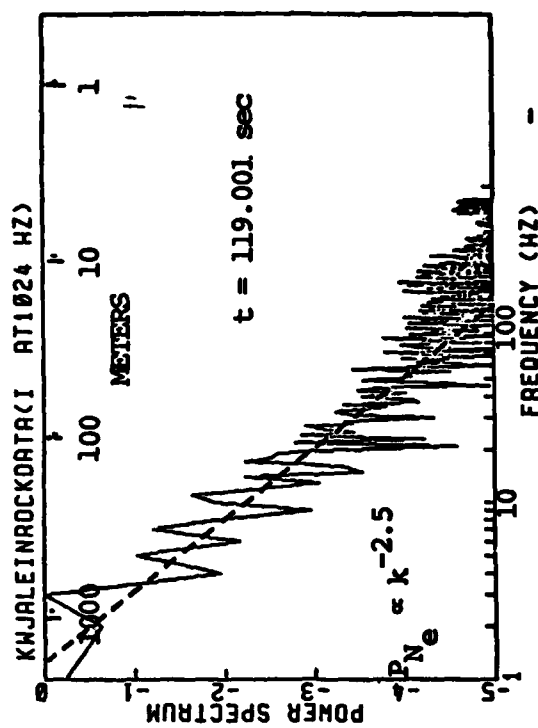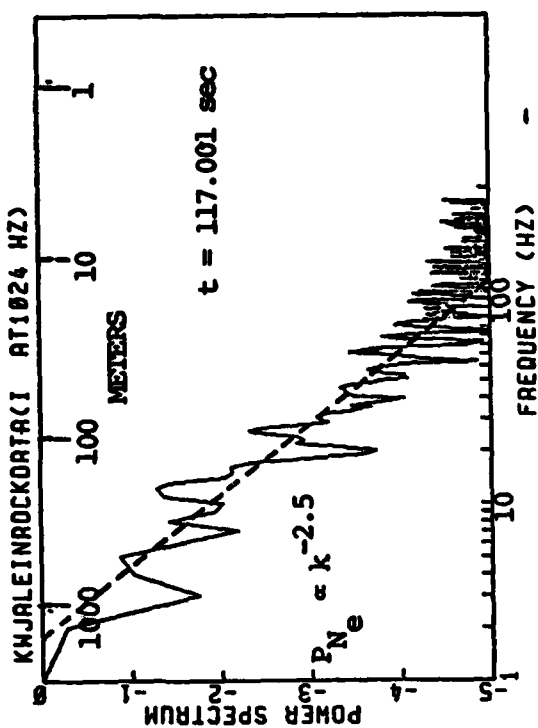
Fig. 9 — Power spectral analyses of density fluctuations in region "C" (Fig. 5)

DISTRIBUTION LIST

DEPARTMENT OF DEFENSE

ASSISTANT SECRETARY OF DEFENSE
COMM, DMD, CONT & INTELL
WASHINGTON, D.C. 20301
    01CY ATTN J. BABCOCK
    01CY ATTN M. EPSTEIN

ASSISTANT TO THE SECRETARY OF DEFENSE
ATOMIC ENERGY
WASHINGTON, D.C. 20301
    01CY ATTN EXECUTIVE ASSISTANT

DIRECTOR
COMMAND CONTROL TECHNICAL CENTER
PENTAGON RM BE 685
WASHINGTON, D.C. 20301
    01CY ATTN C-650
    01CY ATTN C-312 R. MASON

DIRECTOR
DEFENSE ADVANCED RSCH PROJ AGENCY
ARCHITECT BUILDING
1400 WILSON BLVD.
ARLINGTON, VA. 22209
    01CY ATTN NUCLEAR MONITORING RESEARCH
    01CY ATTN STRATEGIC TECH OFFICE

DEFENSE COMMUNICATION ENGINEER CENTER
1860 WIEHLE AVENUE
RESTON, VA. 22290
    01CY ATTN CODE R820
    01CY ATTN CODE R410 JAMES W. MCLEAN
    01CY ATTN CODE R720 J. WORTHINGTON

DEPT. OF THE AIR FORCE
HEADQUARTERS SPACE DIVISION
(AFSC) LOS ANGELES AIR FORCE STATION
P.O. BOX 92960
LOS ANGELES, CA 90009
    01CY DIRECTOR, STP,
      COL D.E. THURSBY
    01CY MAJ C. JUND

DIRECTOR
DEFENSE INTELLIGENCE AGENCY
WASHINGTON, D.C. 20301
    01CY ATTN DT-1B
    01CY ATTN DB-4C E. O'FARRELL
    01CY ATTN DIAAP A. WISE
    01CY ATTN DIAST-5
    01CY ATTN DT-1BZ R. MORTON
    01CY ATTN HQ #-TR J. STEWART
    01CY ATTN W. WITTIG DC-7D

DIRECTOR
DEFENSE NUCLEAR AGENCY
WASHINGTON, D.C. 20305
    01CY ATTN STVL
    04CY ATTN TITL
    01CY ATTN DDST
    03CY ATTN RAAE

COMMANDER
FIELD COMMAND
DEFENSE NUCLEAR AGENCY
KIRTLAND AFB, NM 87115
    01CY ATTN FCPR

DIRECTOR
INTERSERVICE NUCLEAR WEAPONS SCHOOL
KIRTLAND AFB, NM 87115
    01CY ATTN FCPR

DIRECTOR
JOINT STRAT TGT PLANNING STAFF
OFFUTT AFB
OMAHA, NB 68113
    01CY ATTN JLTW-2
    01CY ATTN JPST G. GOETZ

JOINT CHIEFS OF STAFF
WASHINGTON, D.C. 20301
    01CY ATTN J-3 WWMCCS EVALUATION
      OFFICE

CHIEF
LIVERMORE DIVISION FLD COMMAND DNA
DEPARTMENT OF DEFENSE
LAWRENCE LIVERMORE LABORATORY
P.O. BOX 808
LIVERMORE, CA 94550
    01CY ATTN FCPRL

DIRECTOR
NATIONAL SECURITY AGENCY
DEPARTMENT OF DEFENSE
FT. GEORGE G. MEADE, MD 20755
    01CY ATTN JOHN SKILLMAN R52
    01CY ATTN FRANK LEONARD
    01CY ATTN W14 PAT CLARK
    01CY ATTN OLIVER H. BARTLETT W32
    01CY ATTN R5

COMMANDANT
NATO SCHOOL (SHAPE)
APO NEW YORK 09172
    01CY ATTN U.S. DOCUMENTS OFFICER

68-Blank

69

COMMANDER
U.S. ARMY COMM-ELEC ENGRG INSTAL AGY
FT. HUACHUCA, AZ 85613
    01CY ATTN CCC-EMEO GEORGE LANE

COMMANDER
U.S. ARMY FOREIGN SCIENCE & TECH CTR
220 7TH STREET, NE
CHARLOTTESVILLE, VA 22901
    01CY ATTN DRXST-SD
    01CY ATTN R. JONES

COMMANDER
U.S. ARMY MATERIAL DEV & READINESS CMD
5001 EISENHOWER AVENUE
ALEXANDRIA, VA 22333
    01CY ATTN DRCLDC J.A. BENDER

COMMANDER
U.S. ARMY NUCLEAR AND CHEMICAL AGENCY
7500 BACKLICK ROAD
BLDG. 2073
SPRINGFIELD, VA 22150
    01CY ATTN LIBRARY

DIRECTOR
U.S. ARMY BALLISTIC RESEARCH LABS
ABERDEEN PROVING GROUND, MD 21005
    01CY ATTN TECH LIB EDWARD BAICY

COMMANDER
U.S. ARMY SATCOM AGENCY
FT. MONMOUTH, NJ 07703
    01CY ATTN DOCUMENT CONTROL

COMMANDER
U.S. ARMY MISSILE INTELLIGENCE AGENCY
REDSTONE ARSENAL, AL 35809
    01CY ATTN JIM GAMBLE

DIRECTOR
U.S. ARMY TRADOC SYSTEMS ANALYSIS ACTIVITY
WHITE SANDS MISSILE RANGE, NM 88002
    01CY ATTN ATAA-SA
    01CY ATTN TCC/F. PAYAN JR.
    01CY ATTN ATAA-TAC LTC. J. HESSE

COMMANDER
NAVAL ELECTRONIC SYSTEMS COMMAND
WASHINGTON, D.C. 20360
    01CY ATTN NAVLEX 034 T. HUGHES
    01CY ATTN PME 117
    01CY ATTN PME 117-T
    01CY ATTN CODE 5011
    01CY ATTN PME-106-T

UNDER SECY OF DEF FOR RSCH & ENGR.
DEPARTMENT OF DEFENSE
WASHINGTON, D.C. 20301
    01CY ATTN STRATEGIC & SPACE SYSTEMS
        (OS)

WWMCCS SYSTEM ENGINEERING ORG.
WASHINGTON, D.C. 20305
    01CY ATTN R. CRAWFORD

COMMANDER/DIRECTOR
ATMOSPHERIC SCIENCES LABORATORY
U.S. ARMY ELECTRONICS COMMAND
WHITE SANDS MISSILE RANGE, NM 88002
    01CY ATTN DELAS-EO F. NILES

DIRECTOR
BMD ADVANCED TECH CTR
HUNTSVILLE OFFICE
P.O. BOX 1500
HUNTSVILLE, AL 35807
    01CY ATTN ATC-T MELVIN T. CAPPS
    01CY ATTN ATC-O W. DAVIES
    01CY ATTN ATC-R DON RUSS

PROGRAM MANAGER
BMD PROGRAM OFFICE
5001 EISENHOWER AVENUE
ALEXANDRIA, VA 22333
    01CY ATTN DACS-BMT J. SHEA

CHIEF C-E SERVICE DIVISION
U.S. ARMY COMMUNICATIONS CMD
PENTAGON RM. 1B269
WASHINGTON, D.C. 20310
    01CY ATTN C-E-SERVICES DIVISION

COMMANDER
FRADCOM TECHNICAL SUPPORT ACTIVITY
DEPARTMENT OF THE ARMY
FORT MONMOUTH, N.J. 07703
    01CY ATTN DRSEL-NL-RD H. BENNET
    01CY ATTN DRSEL-PL-ENV H. BOMKE
    01CY ATTN J.E. QUIGELY

COMMANDER
HARRY DIAMOND LABORATORIES
DEPARTMENT OF THE ARMY
2800 POWDER MILL ROAD
ADELPHI, MD 20783
        (CNWDI-INNER ENVELOPE: ATTN: DELHD-RBH)
    01CY ATTN DELHD-TI M. WEINER
    01CY ATTN DELHD-RB R. WILLIAMS
    01CY ATTN DELHD-NP F. WIMENITZ
    01CY ATTN DELHD-NP C. MOAZED

```
01CY  CODE 4732 E. MCLEAN          SAMSO/SZ
01CY  CODE 6000                    POST OFFICE BOX 92960
01CY  CODE 7000                    WORLDWAY POSTAL CENTER
01CY  CODE 7500                    LOS ANGELES, CA  90009
01CY  CODE 7580                    (SPACE DEFENSE SYSTEMS)
01CY  CODE 7551                        01CY  ATTN SZJ
01CY  CODE 7555
01CY  CODE 7900                    STRATEGIC AIR COMMAND/XPFS
                                   OFFUTT AFB, NB  68113
COMMANDER                              01CY  ATTN XPFS MAJ B. STEPHAN
NAVAL SEA SYSTEMS COMMAND              01CY  ATTN ADWATE MAJ. BRUCE BAUER
WASHINGTON, D.C.  20362                01CY  ATTN NRT
    01CY  ATTN CAPT. R. PITKIN          01CY  ATTN DOK CHIEF SCIENTIST

COMMANDER                          SAMSO/YA
NAVAL SPACE SURVEILLANCE SYSTEM     P.O. BOX 92960
DAHLGREN, VA  22448                 WORLDWAY POSTAL CENTER
    01CY  ATTN CAPT. J.H. BURTON    LOS ANGELES, CA  90009
                                       01CY  ATTN YAT CAPT L. BLACKWELDER
OFFICER-IN-CHARGE
NAL SURFACE WEAPONS CENTER          SAMSO/SK
WHITE OAK, SILVER SPRING, MD  20910 P.O. BOX  92960
    01CY  ATTN CODE F31             WORLDWAY POSTAL CENTER
                                    LOS ANGELES, CA  90009
DIRECTOR STRATEGIC SYSTEMS PROJECT OFFICE   01CY  ATTN SKA (SPACE COMM SYSTEMS) M. CLAVIN
DEPARTMENT OF THE NAVY
WASHINGTON, D.C.  20376             SAMSO/MN
    01CY  ATTN NSP-2141             NORTON AFB, CA  92409
    01CY  ATTN NSSP-2722 FRED WIMBERLY   (MINUTEMAN)
                                       01CY  ATTN MNNL LTC KENNEDY
NAVAL SPACE SYSTEM ACTIVITY
P.O. BOX  92960                     COMMANDER
WORLDWAY POSTAL CENTER              ROME AIR DEVELOPMENT CENTER, AFSC
LOS ANGELES, CA  90009              HANSCOM AFB, MA  01731
    01CY  ATTN LCDR  DONALD SNODDY      01CY  ATTN EEP A. LORENTZEN
    01CY  ATTN COMMANDING OFFICER
                                   DEPARTMENT OF ENERGY
HEADQUARTERS
ELECTRONIC SYSTEMS DIVISION/DC      DEPARTMENT OF ENERGY
DEPARTMENT OF THE AIR FORCE         ALBUQUERQUE OPERATIONS OFFICE
HANSCOM AFB, MA  01731              P.O. BOX 5400
    01CY  ATTN DCKC MAJ J.C. CLARK  ALBUQUERQUE, NM  87115
                                       01CY  ATTN DOC CON FOR D. SHERWOOD
COMMANDER
FOREIGN TECHNOLOGY DIVISION, AFSC   DEPARTMENT OF ENERGY
WRIGHT-PATTERSON AFB, OH  45433     LIBRARY ROOM G-042
    01CY  ATTN NICD LIBRARY         WASHINGTON, D.C.  20545
    01CY  ATTN ETDP B. BALLARD          01CY  ATTN DOC CON FOR A. LABOWITZ

COMMANDER                          EG&G, INC.
ROME AIR DEVELOPMENT CENTER, AFSC   LOS ALAMOS DIVISION
GRIFFISS AFB, NY  13441             P.O. BOX 809
    01CY  ATTN DOC LIBRARY/TSLD     LOS ALAMOS, NM  85544
    01CY  ATTN OCSE V. COYNE            01CY  ATTN DOC CON FOR J. BREEDLOVE
```

UNIVERSITY OF CALIFORNIA
LAWRENCE LIVERMORE LABORATORY
P.O. BOX 808
LIVERMORE, CA 94550
    01CY ATTN DOC CON FOR TECH INFO DEPT
    01CY ATTN DOC CON FOR L-389 R. OTT
    01CY ATTN DOC CON FOR L-31 R. HAGER
    01CY ATTN DOC CON FOR L-46 F. SEWARD

LOS ALAMOS SCIENTIFIC LABORATORY
P.O. BOX 1663
LOS ALAMOS, NM 87545
    01CY ATTN DOC CON FOR J. WOLCOTT
    01CY ATTN DOC CON FOR R.F. TASCHEK
    01CY ATTN DOC CON FOR E. JONES
    01CY ATTN DOC CON FOR J. MALIK
    01CY ATTN DOC CON FOR R. JEFFRIES
    01CY ATTN DOC CON FOR J. ZINN
    01CY ATTN DOC CON FOR P. KEATON
    01CY ATTN DOC CON FOR D. WESTERVELT
    01CY ATTN DOC CON FOR M. PONGRATZ

SANDIA LABORATORIES
P.O. BOX 5800
ALBUQUERQUE, NM 87115
    01CY ATTN DOC CON FOR J. MARTIN
    01CY ATTN DOC CON FOR W. BROWN
    01CY ATTN DOC CON FOR A. THORNBROUGH
    01CY ATTN DOC CON FOR T. WRIGHT
    01CY ATTN DOC CON FOR D. DAHLGREN
    01CY ATTN DOC CON FOR 3141
    01CY ATTN DOC CON FOR SPACE PROJECT DIV

SANDIA LABORATORIES
LIVERMORE LABORATORY
P.O. BOX 969
LIVERMORE, CA 94550
    01CY ATTN DOC CON FOR B. MURPHY
    01CY ATTN DOC CON FOR T. COOK

OFFICE OF MILITARY APPLICATION
DEPARTMENT OF ENERGY
WASHINGTON, D.C. 20545
    01CY ATTN DOC CON FOR D. GALE

OTHER GOVERNMENT

CENTRAL INTELLIGENCE AGENCY
ATTN RD/SI, RM 5G48, HQ BLDG
WASHINGTON, D.C. 20505
    01CY ATTN OSI/PSID RM 5F 19

DEPARTMENT OF COMMERCE
NATIONAL BUREAU OF STANDARDS
WASHINGTON, D.C. 20234
    (ALL CORRES: ATTN SEC OFFICER FOR)
    01CY ATTN R. MOORE

DEPARTMENT OF TRANSPORTATION
OFFICE OF THE SECRETARY
TAD-44.1, ROOM 10402-B
400 7TH STREET, S.W.
WASHINGTON, D.C. 20590
    01CY ATTN R. LEWIS
    01CY ATTN R. DOHERTY

INSTITUTE FOR TELECOM SCIENCES
NATIONAL TELECOMMUNICATIONS & INFO ADMIN
BOULDER, CO 80303
    01CY ATTN A. JEAN (UNCLASS ONLY)
    01CY ATTN W. UTLAUT
    01CY ATTN D. CROMBIE
    01CY ATTN L. BERRY

NATIONAL OCEANIC & ATMOSPHERIC ADMIN
ENVIRONMENTAL RESEARCH LABORATORIES
DEPARTMENT OF COMMERCE
BOULDER, CO 80302
    01CY ATTN R. GRUBB
    01CY ATTN AERONOMY LAB G. REID

DEPARTMENT OF DEFENSE CONTRACTORS

AEROSPACE CORPORATION
P.O. BOX 92957
LOS ANGELES, CA 90009
    01CY ATTN I. GARFUNKEL
    01CY ATTN T. SALMI
    01CY ATTN V. JOSEPHSON
    01CY ATTN S. BOWER
    01CY ATTN N. STOCKWELL
    01CY ATTN D. OLSEN
    01CY ATTN J. CARTER
    01CY ATTN F. MORSE
    01CY ATTN SMFA FOR PWW
    01CY ATTN J. FENNEL
    01CY ATTN C. RICE
    01CY ATTN H. KOONS

ANALYTICAL SYSTEMS ENGINEERING CORP
5 OLD CONCORD ROAD
BURLINGTON, MA 01803
    01CY ATTN RADIO SCIENCES

BERKELEY RESEARCH ASSOCIATES, INC.
P.O. BOX 983
BERKELEY, CA 94701
    01CY ATTN J. WORKMAN

BOEING COMPANY, THE
P.O. BOX 3707
SEATTLE, WA 98124
    01CY ATTN G. KEISTER
    01CY ATTN D. MURRAY
    01CY ATTN G. HALL
    01CY ATTN J. KENNEY

CALIFORNIA AT SAN DIEGO, UNIV OF
IPAPS, B-019
LA JOLLA, CA 92093
    01CY ATTN HENRY G. BOOKER
    01CY ATTN E.C. WHIPPLE

BROWN ENGINEERING COMPANY, INC.
CUMMINGS RESEARCH PARK
HUNTSVILLE, AL 35807
    01CY ATTN ROMEO A. DELIBERIS

CHARLES STARK DRAPER LABORATORY, INC.
555 TECHNOLOGY SQUARE
CAMBRIDGE, MA 02139
    01CY ATTN D.B. COX
    01CY ATTN J.P. GILMORE

COMPUTER SCIENCES CORPORATION
6565 ARLINGTON BLVD
FALLS CHURCH, VA 22046
    01CY ATTN H. BLANK
    01CY ATTN JOHN SPOOR
    01CY ATTN C. NAIL

COMSAT LABORATORIES
LINTHICUM ROAD
CLARKSBURG, MD 20734
    01CY ATTN G. HYDE

ELECTROSPACE SYSTEMS, INC.
BOX 1359
RICHARDSON, TX 75080
    01CY ATTN H. LOGSTON
    01CY ATTN SECURITY (PAUL PHILLIPS)

ESL INCL.
495 JAVA DRIVE
SUNNYVALE, CA 94086
    01CY ATTN J. ROBERTS
    01CY ATTN JAMES MARSHALL
    01CY ATTN C.W. PRETTIE

FORD AEROSPACE AND COMMUNICATIONS CORP
3939 FABIAN WAY
PALO ALTO, CA 94303
    01CY ATTN J.T. MATTINGLEY

GENERAL ELECTRIC COMPANY
SPACE DIVISION
VALLEY FORGE SPACE CENTER
GODDARD BLVD KING OF PRUSSIA
P.O. BOX 8555
PHILADELPHIA, PA 19101
    01CY ATTN M.H. BORTNER SPACE SCI LAB

GENERAL ELECTRIC COMPANY
P.O. BOX 1122
SYRACUSE, NY 13201
    01CY ATTN F. REIBERT

GENERAL ELECTRIC COMPANY
TEMPO-CENTER FOR ADVANCED STUDIES
816 STATE STREET (P.O. DRAWER QQ)
SANTA BARBARA, CA 93102
    01CY ATTN DASIAC
    01CY ATTN DON CHANDLER
    01CY ATTN TOM BARRETT
    01CY ATTN TIM STEPHANS
    01CY ATTN WARREN S. KNAPP
    01CY ATTN WILLIAM MCNAMARA
    01CY ATTN B. GAMBILL
    01CY ATTN MACK STANTON

GENERAL ELECTRIC TECH SERVICES CO., INC.
HMES
COURT
SYRACUSE, NY 13201
    01CY ATTN G. MILLMAN

GENERAL RESEARCH CORPORATION
SANTA BARBARA DIVISION
P.O. BOX 6770
SANTA BARBARA, CA 93111
    01CY ATTN JOE ISE JR
    01CY ATTN JOEL GARBARINO

GEOPHYSICAL INSTITUTE
UNIVERSITY OF ALASKA
FAIRBANKS, AK 99701
    (ALL CLASS ATTN: SECURITY OFFICERS)
    01CY ATTN T.N. DAVIS (UNCL ONLY)
    01CY ATTN NEAL BROWN (UNCL ONLY)
    01CY ATTN TECHNICAL LIBRARY
    01CY ATTN T. HALLINAN

74

GTE SYLVANIA, INC.
ELECTRONICS SYSTEMS GRP-EASTERN DIV
77 - STREET
NEEDHAM, MA 02194
01CY ATTN MARSHAL CROSS

ILLINOIS, UNIVERSITY OF
DEPARTMENT OF ELECTRICAL ENGINEERING
URBANA, IL 61803
01CY ATTN K. YEH

INSTITUTE FOR DEFENSE ANALYSES
400 ARMY-NAVY DRIVE
ARLINGTON, VA 22202
01CY ATTN J.M. AEIN
01CY ATTN HANS WOLFHARD
01CY ATTN JOEL BENGSTON

HSS, INC.
2 ALFRED CIRCLE
BEDFORD, MA 01730
01CY ATTN DONALD HANSEN

INTL TEL & TELEGRAPH CORPORATION
500 WASHINGTON AVENUE
NUTLEY, NJ 07110
01CY ATTN TECHNICAL LIBRARY

JAYCOR
1401 CAMINO DEL MAR
DEL MAR, CA 92014
01CY ATTN S.R. GOLDMAN

JOHNS HOPKINS UNIVERSITY
APPLIED PHYSICS LABORATORY
JOHNS HOPKINS ROAD
LAUREL, MD 20810
01CY ATTN DOCUMENT LIBRARIAN
01CY ATTN THOMAS POTEMRA
01CY ATTN JOHN DASSOULAS

LOCKHEED MISSILES & SPACE CO INC
P.O. BOX 504
SUNNYVALE, CA 94088
01CY ATTN DEPT 60-12
01CY ATTN D.R. CHURCHILL

LOCKHEED MISSILES AND SPACE CO INC
3251 HANOVER STREET
PALO ALTO, CA 94304
01CY ATTN MARTIN WALT DEPT 52-10
01CY ATTN RICHARD G. JOHNSON DEPT 52-12
01CY ATTN W.L. IMHOF DEPT 52-12
01CY ATTN D. CAUFMAN

KAMAN SCIENCES CORP
P.O. BOX 7463
COLORADO SPRINGS, CO 80933
01CY ATTN T. MEAGHER

LINKABIT CORP
10453 ROSELLE
SAN DIEGO, CA 92121
01CY ATTN IRWIN JACOBS
01CY ATTN I. ROTHMUELLER

LOWELL RSCH FOUNDATION, UNIVERSITY OF
450 AIKEN STREET
LOWELL, MA 01854
01CY ATTN K. BIBL
01CY ATTN B. REINISCH

M.I.T. LINCOLN LABORATORY
P.O. BOX 73
LEXINGTON, MA 02173
01CY ATTN DAVID M. TOWLE
01CY ATTN P. WALDRON
01CY ATTN L. LOUGHLIN
01CY ATTN D. CLARK
01CY ATTN J. DAVIS

MARTIN MARIETTA CORP
ORLANDO DIVISION
P.O. BOX 5837
ORLANDO, FL 32805
01CY ATTN R. HEFFNER

MCDONNELL DOUGLAS CORPORATION
5301 BOLSA AVENUE
HUNTINGTON BEACH, CA 92647
01CY ATTN N. HARRIS
01CY ATTN J. MOULE
01CY ATTN GEORGE MROZ
01CY ATTN W. OLSON
01CY ATTN R.W. HALPRIN
01CY ATTN TECHNICAL LIBRARY SERVICES

MISSION RESEARCH CORPORATION
735 STATE STREET
SANTA BARBARA, CA 93101
01CY ATTN P. FISCHER
01CY ATTN W.F. CREVIER
01CY ATTN STEVEN L. GUTSCHE
01CY ATTN D. SAPPENFIELD
01CY ATTN R. BOGUSCH
01CY ATTN RALPH KILB
01CY ATTN R. HENDRICK
01CY ATTN DAVE SOWLE
01CY ATTN F. FAJEN
01CY ATTN N. SCHEIBE
01CY ATTN CONRAD L. LONGMIRE
01CY ATTN WARREN A. SCHLUETER

MITRE CORPORATION, THE
P.O. BOX 208
BEDFORD, MA 01730
     01CY ATTN JOHN MORGANSTERN
     01CY ATTN G. HARDING
     01CY ATTN C.E. CALLAHAN

MITRE CORP
WESTGATE RESEARCH PARK
1820 DOLLY MADISON BLVD
MCLEAN, VA 22101
     01CY ATTN W. HALL
     01CY ATTN W. FOSTER

PACIFIC-SIERRA RESEARCH CORP
1456 CLOVERFIELD BLVD.
SANTA MONICA, CA 90404
     01CY ATTN E.C. FIELD JR

PENNSYLVANIA STATE UNIVERSITY
IONISPHERE RESEARCH LAB
318 ELECTRICAL ENGINEERING EAST
UNIVERSITY PARK, PA 16802
     (NO CLASSIFIED TO THIS ADDRESS)
     01CY ATTN IONOSPHERIC RESEARCH LAB

PHOTOMETRICS, INC.
442 MARRETT ROAD
LEXINGTON, MA 02173
     01CY ATTN IRVING L. KOFSKY

PHYSICAL DYNAMICS INC.
P.O. BOX 3027
BELLEVUE, WA 98009
     01CY ATTN E.J. FREMOUW

PHYSICAL DYNAMICS INC.
P.O. BOX 1069
BERKELEY, CA 94701
     01CY ATTN A. THOMPSON

R & D ASSOCIATES
P.O. BOX 9695
MARINA DEL REY, CA 90291
     01CY ATTN FORREST GILMORE
     01CY ATTN BRYAN GABBARD
     01CY ATTN WILLIAM B. WRIGHT JR.
     01CY ATTN WILLIAM J. KARZAS
     01CY ATTN ROBERT F. LELEVIER
     01CY ATTN H. ORY
     01CY ATTN C. MACDONALD
     01CY ATTN R. TURCO

RAND CORPORATION, THE
1700 MAIN STREET
SANTA MONICA, CA 90406
     01CY ATTN CULLEN CRAIN
     01CY ATTN ED BEDROZIAN

RIVERSIDE RESEARCH INSTITUTE
80 WEST END AVENUE
NEW YORK, NY 10023
     01CY ATTN VINCE TRAPANI

SCIENCE APPLICATION, INC.
P.O. BOX 2351
LAJOLLA, CA 92038
     01CY ATTN LEWIS M. LINSON
     01CY ATTN DANIEL A. HAMLIN
     01CY ATTN D. SACHS
     01CY ATTN E.A. STRAKER
     01CY ATTN CURTUS A. SMITH
     01CY ATTN JACK MCDOUGALL

RAYTHEON CO.
528 BOSTON POST ROAD
SUDBURY, MA 01776
     01CY ATTN BARBARA ADAMS

SCIENCE APPLICATIONS, INC.
HUNTSVILLE DIVISION
2109 W. CLINTON AVENUE
SUITE 700
HUNTSVILLE, AL 35805
     01CY ATTN DALE H. DAVIS

SCIENCE APPLICATIONS, INCORPORATED
8400 WESTPARK DRIVE
MCLEAN, VA 22101
     01CY ATTN J. COCKAYNE

SCIENCE APPLICATIONS, INC.
80 MISSION DRIVE
PLEASANTON, CA 94566
     01CY ATTN SZ

SRI INTERNATIONAL
333 RAVENSWOOD AVENUE
MENLO PARK, CA 94025
     01CY ATTN DONARD NEILSON
     01CY ATTN ALAN BURNS
     01CY ATTN G. SMITH
     01CY ATTN L.L. COBB
     01CY DAVID A. JOHNSON
     01CY ATTN WALTER G. CHESNUT
     01CY ATTN CHARLES L. RINO
     01CY ATTN WALTER JAYE
     01CY ATTN N. BARON
     01CY ATTN R. LIVINGSTON

```
                    01CY  ATTN RAY L. LEADABRAND
                    01CY  ATTN C. CARPENTER
                    01CY  ATTN G. PRICE
                    01CY  ATTN J. PETERSON
                    01CY  ATTN R. HAKE, JR.
                    01CY  ATTN V. GONZALES
                    01CY  ATTN D. MCDANIEL
                    01CY  ATTN R. TSUNODA

TECHNOLOGY INTERNATIONAL CORP
75 WIGGINS AVENUE
BEDFORD, MA  01730
        01CY  ATTN W.P. BOQUIST

UNIVERSITY OF TOKYO
ISAS
KOMABA, MEGURO-KU
TOKYO, JAPAN
        01CY  ATTN  DR. K.I. OYAMA

MAX-PLANCK-INSTITUT
FUR PHYSIK UND ASTROPHYSIK
INSTITUT FUR EXTRATERRESTRICHE PHYSIK
8046 GARCHING B. MUNCHEN, GERMANY
        01CY  ATTN PROF. GERHARD HAERENDEL


TRW DEFENSE & SPACE SYS GROUP
ONE SPACE PARK
REDONDO BEACH, CA  90278
        01CY  ATTN R.K. PLEBUCH
        01CY  ATTN S. ALTSCHULER
        01CY  ATTN D. DEE

VISIDYNE, INC.
19 THIRD AVENUE
NORTH WEST INDUSTRIAL PARK
BURLINGTON, MA  01802
        01CY  ATTN CHARLES HUMPHREY
        01CY  ATTN J.W. CARPENTER
```

PLEASE DISTRIBUTE ONE COPY (EXCEPT WHERE NOTED
OTHERWISE) TO EACH OF THE FOLLOWING PEOPLE:

ADVANCED RESEARCH PROJECTS AGENCY (ARPA)
STRATEGIC TECHNOLOGY OFFICE
ARLINGTON, VA 22217

    CAPT DONALD M. LEVINE

NAVAL RESEARCH LABORATORY
WASHINGTON, D.C. 20375

    DR. R. MEIER - CODE 4141
    DR. TIMOTHY COFFEY - CODE 4000
    DR. S. OSSAKOW - CODE 4780
    DR. J. GOODMAN - CODE 4180
    DR. E. SZUSZCZEWICZ - CODE 4187 (50 COPIES)

DIRECTOR OF SPACE AND ENVIRONMENTAL LABORATORY
NOAA
BOULDER, CO 80302

    DR. A. GLENN JEAN
    DR. G. W. ADAMS
    DR. D. N. ANDERSON
    DR. K. DAVIES
    DR. R. F. DONNELLY

AIR FORCE GEOPHYSICS LABORATORY
HANSCOM AIR FORCE BASE, MA 01731

    DR. T. ELKINS
    DR. W. SWIDER
    MRS. R. SAGALYN
    DR. J. M. FORBES
    DR. T. J. KENESHEA
    DR. J. AARONS
    DR. R. NARCISI

OFFICE OF NAVAL RESEARCH
800 NORTH QUINCY STREET
ARLINGTON, VA 22217

U.S. ARMY ABERDEEN RESEARCH AND DEVELOPMENT
CENTER BALLISTIC RESEARCH LABORATORY
ABERDEEN, MD 21001

    DR. J. HEIMERL

COMMANDER
NAVAL AIR SYSTEMS COMMAND
DEPARTMENT OF THE NAVY
WASHINGTON, D.C. 20360

    DR. T. CZUBA

HARVARD UNIVERSITY
HARVARD SQUARE
CAMBRIDGE, MASS. 02138

    DR. M. B. McELROY
    DR. R. LINDZEN

PENNSYLVANIA STATE UNIVERSITY
UNIVERSITY PARK, PA 16802

    DR. J. S. NISBET
    DR. P. R. ROHRBAUGH
    DR. D. E. BARAN
    DR. L. A. CARPENTER
    DR. M. LEE
    DR. R. DIVANY
    DR. P. BENNETT
    DR. E. KLEVANS

UNIVERSITY OF CALIFORNIA, LOS ANGELES
405 HILLGARD AVENUE
LOS ANGELES, CA 90024

    DR. R. STENZEL
    DR. F. V. CORONITI
    DR. C. KENNEL
    DR. W. GEKELMAN

UNIVERSITY OF CALIFORNIA, BERKELEY
BERKELEY, CA 94720

    DR. M. HUDSON

UTAH STATE UNIVERSITY
4TH AND 8TH STREETS
LOGAN, UTAH 84322

    DR. P. M. BANKS
    DR. R. HARRIS
    DR. V. PETERSON
    DR. R. MEGILL
    DR. K. BAKER
    DR. R. WILLIAMSON

CORNELL UNIVERSITY
ITHACA, N.Y. 14850

DR. W. E. SWARTZ
DR. R. SUDAN
DR. D. FARLEY
DR. M. KELLEY

NASA
GODDARD SPACE FLIGHT CENTER
GREENBELT, MD 20771

DR. S. J. BAUER/CODE 600
DR. R. HARTEL/CODE 621
DR. R. GOLDBERG/CODE 912
DR. S. CHANDRA
DR. K. MAEDO
DR. R. BENSON/CODE 621

PRINCETON UNIVERSITY
PLASMA PHYSICS LABORATORY
PRINCETON, N.J. 08540

DR. F. PERKINS
DR. E. FRIEMAN

INSTITUTE FOR DEFENSE ANALYSIS
400 ARMY/NAVY DRIVE
ARLINGTON, VA 22202

DR. E. BAUER

UNIVERSITY OF MARYLAND
COLLEGE PARK, MD 20742

DR. K. PAPADOPOULOS
DR. E. OTT

UNIVERSITY OF PITTSBURGH
PITTSBURGH, PA 15213

DR. N. ZABUSKY
DR. M. BIONDI

DEFENSE DOCUMENTATION CENTER
CAMERON STATION
ALEXANDRIA, VA 22314

(12 COPIES IF OPEN PUBLICATION
OTHERWISE 2 COPIES) 12 CY ATTN TC

UNIVERSITY OF CALIFORNIA
LOS ALAMOS SCIENTIFIC LABORATORY
J-10, MS-664
LOS ALAMOS, NEW MEXICO 87545

DR. M. PONGRATZ
DR. D. SIMONS
DR. G. BARASCH
DR. L. DUNCAN

OFFICE OF ASSISTANT SECRETARY OF NAVY
 FOR RESEARCH, ENGINEERING AND SYSTEMS
PENTAGON RM 4D745
Washington, DC 20350

03 CY Attn Dr. H. Rabin
Deputy Assistant
Sec. of Navy